8-2017

Numerical Analysis of Energy Harvesting Process Using Piezoelectric Transducers in an Oscillating Heat Pipe

Sajiree Vaidya
Clemson University, sajirev@clemson.edu

NUMERICAL ANALYSIS OF ENERGY HARVESTING PROCESS USING PIEZOELECTRIC TRANSDUCERS IN AN OSCILLATING HEAT PIPE

A Thesis
Presented to
the Graduate School of
Clemson University

In Partial Fulfillment
of the Requirements for the Degree
Master of Science
Mechanical Engineering

---

by
Sajiree Vaidya
August 2017

Accepted by:
Dr.Oliver Myers, Committee Chair
Dr. Suyi Li
External Honorary Committee Member:
Dr. Scott Thompson
Auburn State University

ABSTRACT

Energy harvesting is a powerful process that deals with exploring different possible ways of converting energy dispersed in the environment into useful form of energy, essentially electrical energy. Piezoelectric materials are known for their ability of transferring mechanical energy into electrical energy or vice versa. This work takes an advantage of piezoelectric material's properties to covert thermal energy into electrical energy in an oscillating heat pipe. Specific interest in an oscillating heat pipe has relevance to energy harvesting for low power generation suitable for remote electronics operation as well as low-power heat reclamation for electronic packaging.

The aim of this research is to develop a multi-physics numerical analysis model that aids in predicting electrical power generation inherent to an oscillating heat pipe. The experimental design consists of a piezoelectric patch with fixed configuration, attached inside an oscillating heat pipe and its behavior when subjected to the oscillating fluid pressure was observed. Numerical analysis of the model depicting the similar behavior was developed using COMSOL multi physics FEA software. The numerical model consists of a three-way physics interaction that takes into account thermo-hydrodynamic interaction, fluid-structure interaction, and piezoelectric effect. Results obtained from 3D numerical analysis are compared with experimental recordings to validate the numerical model.

DEDICATION

. कर्मण्येवाधिकारस्ते मा फलेषु कदाचन।

मा कर्मफलहेतुर्भूर्मा ते सङ्गोऽस्त्वकर्मणि॥

२-४७ [Bhagwad Gita]

Meaning —You have the right to work only but never to its fruits. Let not the fruits of action be your motive, nor let your attachment be to inaction.

This thesis is dedicated to my family for teaching me to let my efforts lead my life.

ACKNOWLEDGMENTS

I would like to express my sincere gratitude to my principal advisor Dr. Oliver J. Myers for his constant guidance and encouragement, and for giving me this wonderful opportunity to learn and explore the engineer in me. I am truly grateful for his unwavering support throughout my Masters.

I am thankful to Dr. Scott Thompson for his guidance through this research. I am also thankful to Dr. Suyi Li for his support for this work.

I am thankful to the faculty and staff in the Department of Mechanical Engineering, especially Ms. Trish Nigro for the support towards successful completion of my graduate studies at Clemson University.

I also acknowledge the support and encouragement given by my family, friends and graduate alumni students, which helped me complete my thesis and Masters in Mechanical Engineering.

This research was supported by the NSF EAGER: Energy harvesting via Thermo-piezoelectric Transduction Grant # 1549973.

TABLE OF CONTENTS

Page

Page

LIST OF TABLES

Page

LIST OF FIGURES

Page

Page

CHAPTER ONE

INTRODUCTION

Considerable amount of waste heat is generated within variety of working environment. Environments containing temperature gradients and heat flow have the potential to generate electrical power through thermoelectric energy conversion. The temperature difference provides the potential for efficient energy conversion, and the heat flow provides the power [1]. Passive methods of energy harvesting by converting heat flux into electrical energy have been continuously explored. However, the power output from such system is low due to low Carnot and material efficiency. A thermally reliant and passive energy harvesting system combined with thermal management system can serve as an effective solution to this problem.

Oscillating heat pipe (OHP) is a two-phase heat transfer device that relies on the oscillatory flow of liquid slug and vapor plug in along miniature tube bent in several turns [2]. With a sufficient temperature difference imposed across the OHP, the internal fluid vaporizes due to heat transfer between the evaporator and condenser section. This induces a non-uniform pressure distribution inside the channel structure that gives rise to an oscillatory flow pattern. OHP is extensively investigated for their ability of serving as a power reclamation. Available waste heat can be provided as an input to the OHP which will result in oscillatory flow inside the pipe. A piezoelectric material patch, placed in an adiabatic section of the OHP, deforms under fluid oscillations. This results in creating

stress in the material, thereby generating electrical energy as an output. The main advantage of this approach is the possibility of low-power generation suitable for remote or logistically weak electronics applications as well as low-power heat reclamation for electronics, providing a compact means to mitigate and recover waste heat for eventual reuse.

In chapter 2, the literature review is carried out to explain the research efforts undertaken by researchers in this area and the outcome of their work. It also points out a gap in the existing available solution which will be addressed by our work. Chapter 3 deals with theoretical approach of the work which explains the theory behind multiple physics coupled in this work. In chapter 4, the experiments employed for this research are explained in detail which serve as a baseline for the numerical model considerations and set-up. Chapter 5 explains the numerical analysis approach developed to generate required pressure boundary conditions using MATLAB, inherent to the OHP. Chapters 6 deals with the numerical approach along with development of the FEA model with relevant equations, meshing details, pre and post- processing methods, and results of the numerical model.

Chapter 7 includes the conclusions of this research, reasons for the observed variations and the future work/extensions of this research.

CHAPTER TWO

LITERATURE REVIEW

In 1799, Alexander Volta gifted us with world's first practical electricity source in the form of a battery. Despite vacuum tube electronics' weight and large associated battery, people living in the early 1900s enjoyed their off the power grid picnics with enormous portable radios [3]. Technology growth gave rise to smaller electronics and enabled today's wireless and mobile applications explosion. With ever increasing demand of energy, it has become extremely important to efficiently generate and store the useful form of energy. It is equally important to reuse the available waste energy by applying suitable techniques. For this reason, researchers started to explore various techniques of energy harvesting.

Energy harvesting methods of obtaining electrical energy from the ambient surrounding energy have been largely investigated for its ability to reuse the waste energy available in abundance. One of such popular area of research is ambient energy harvesting to enable self powered wireless electronic systems [4].

Environmental power sources for energy harvesting include mechanical vibrations, light, heat and electromagnetic radiation. Ambient light presents an opportunity to scavenge power using an inexpensive crystalline silicon solar cell [3]. These products can harness light as an energy source in a range of kilowatts on a bright sunny day. But the use of this application is limited by the necessity of consistent sunlight.

Vibrational excitation provides a useful means of recovering the waste energy. This mode can be broadly classified into mechanical vibration excitation, human powered energy generation and fluid vibration induced excitation. Mechanical vibrations fall in a varied and wide range depending on the frequency and amplitude of vibrations. These include floor vibration of machine shop to severe vibrations caused due to engine operation. Several methods exists for obtaining electrical energy from vibrational excitation. Use of electromagnetic induction principle using moving coil around magnets and piezoelectric materials are some notable methods in this category [5] [6] [7]. While each of the aforementioned techniques can provide a useful amount of energy, piezoelectric materials have received the most attention. This is due to their ability to directly convert applied strain energy into usable electric energy and the ease at which they can be integrated into a system [4]. A large percentage of recent research has been focused on improving the efficiency of piezoelectric energy harvesting systems. Piezoelectric material has a significant influence in harvester's functionality and performance. Piezoceramic (PZT), polyvinylidene fluoride (PVDF) and Macro-Fiber Composite (MFC) are one of the widely used piezoelectric materials for the purpose of energy harvesting. A comparative study in between PZT, quick pack actuator and MFC shows that PZT was found to be the most effective material to cater random ambient vibrations [8], whereas MFC performance is found to be excellent as a sensor as well as an actuator when tested for energy harvesting purpose [9][10]. Piezoelectric coupling mode is another effective parameter affecting energy harvesting capability. In -31 mode, force is applied in the direction perpendicular to the poling directions whereas in -33 mode force is applied in the same direction as the

poling direction. Conventionally, the -31 mode is the most commonly used coupling mode, as the resonant frequency of a system operating in -31 mode is much lower making the system capable of being driven at resonance in natural environment [11]. Optimizing the design of piezoelectric patch provides another means of increasing efficiency of the harvester. Effectiveness of the piezoelectric design was found to be dependent on the damping ratio and coupling coefficient [12]. Output voltage is seen to be maximum when the resonant frequency of the piezoelectric device matches with the frequency of ambient vibrations. It is often noticed that the frequency of ambient vibrations is very low. Hence, self-tuning piezoelectric device was designed which would attain resonant frequency with passive or active power excitation to the piezoelectric cantilever beam [13].

Biomechanical energy harvesting technique is explored to study effective human body movements to possibly harvest energy due to various body movements. It was found out that harvesting the energy obtained through a heel strike is the most useful form of biomechanical energy harvesting followed by ankle and knee movements [14]. Due to the ease of incorporation of the energy harvesting device in the shoe, piezoelectric beam structures as shoe inserts were heavily explored [15] [16]. Wrist movements while walking generate a low frequency motion. Hence, a non-resonant system was proposed for capturing the energy generated through wrist movements [17]. However, achievable power levels through this approach lie in the range of a few milliwatts, which limits the range of devices that can be powered by this method. Efficiency of energy harvesting devices capturing human body motions largely depends on power processing and control circuitry. To enhance usefulness of biomechanical energy conversion, maximum power point

tracking solutions are being explored along with integrated design of the complex wireless system.

Possibility of converting energy from ambient fluid flows into useful electrical energy opens another important avenue to energy harvesting efforts. Like earlier mentioned methods, this method also uses vibration of the piezoelectric material to generate electrical energy but converts fluid flow into vibration through vortices, oscillating flows, and rotational energy. Two major areas of fluid flow energy conservation are wind energy and flow energy conservation. Wind energy has been explored as a traditional renewable energy resource to generate electricity using windmills. However, this approach differs from using wind pressure as a means of creating strain in the piezoelectric material for the purpose of energy harvesting. Wind-stressed piezoelectric cantilever beam has been proven to be a potential energy harvesting technique [18]. An analytical model of energy harvesting using piezoelectric windmill claims that power in the range of 10 milliwatts can be harvested at the wind speed of 10mph, making it a viable solution to capture wind pressure energy [19]. MEMS generator when interacted with surrounding gas can also be used as a wireless sensor for applications like tire pressure sensing mechanism [20]. Flowing water is another important source that can be used in energy harvesting applications. Along with its application in hydroelectric power plants, fluid flow energy can also be used for energy harvesting purpose by submerging piezoelectric materials in the fluid flow. Various ways of placements and structures of piezoelectric material in the fluid stream have been explored to analyze effective ways of harvesting the fluid energy. A piezoelectric patch deforms by the vortices when a bluff body is placed in front of it.

The pressure differential enables the piezoelectric to wave and deform from its original shape generating electricity [21] [22] [23]. It was found out that a triangular bluff body increases the vortex induced vibrations resulting in higher electrical output [24]. Unsteady turbulent flows can be used for flow kinetic energy harvesting when fluid flow with high Reynolds's number is exerting pressure on the piezoelectric material placed in the turbulent boundary layer [25]. Another approach of using hydraulic pressure fluctuations involves placing a piezoelectric stack on an elastic diaphragm that absorbs pressure fluctuations from the hydraulic system. This is an effective method of energy harvesting with higher power output despite off –resonance stack excitation [26].

Thermoelectric conversion provides another opportunity of energy harvesting by converting waste energy into useful electrical energy. Heat transfer in between environments at different temperatures can be used to reuse the waste heat. However, using temperature gradient to harvest the heat energy has some limitations as explained by Carnot cycle. Applications that make use of thermo-mechanical conversion as their power source are designed to run on a lesser amount of energy [27] Any fluctuation in the ambient temperature is likely to change the voltage output of the system. A wristwatch designed by Seiko is a good example of a product that runs on the heat generated by the human body[28]. Due to the limitation posed by the need of power conditioning circuitry, the use of ambient temperature gradient for the purpose of energy harvesting is not completely explored [29]. On a broader aspect, thermal gradients are used in geothermal power stations to generate electricity [30]. Heat pipe is operated on a similar principal which uses temperature gradient resulting in the heat transfer process. In 1990, a special purpose heat

pipe called as oscillating heat pipe (OHP) was invented enabling separation of liquid and vapor flows inside a heat pipe [31]. This was a solution to overcome limitations inherent to traditional heat pipes. In an OHP, thermal energy is provided as an input to the evaporator section resulting in liquid-vapor phase fluid flow travelling to and fro in between evaporator section and condenser section. This gives rise to oscillatory flow due to continuous pressure differential. Heat transfer capacity of an OHP was used for waste heat recovery in HVAC systems [32]. Its potential of energy harvesting was also explored in applications like air preheater and solar collector to harvest the energy from drying process or sunlight. [33][34]. However, another advantage of an oscillating heat pipe is the generation of oscillatory flow of multiphase fluid, which is relatively unexplored. This research gap generates a need of studying the potential of an OHP to produce the oscillations in the fluid which can be used for the purpose of energy harvesting. As discussed in the earlier section, piezoelectric material is proven to be a popular choice to convert various sources of vibrational excitations including fluid flow energy into electrical energy.

With the aim of integrating properties of an OHP and piezoelectric material, this work proposes a new concept of harvesting the energy of oscillatory flow generated inside an OHP using a piezoelectric material placed in the path of the fluid oscillations.

CHAPTER THREE

THEORETICAL APPROACH

3.1 Conceptual Scope

The aim of this work is to predict the voltage output of the energy harvesting system based on given input of the form of thermal energy. For this purpose, it is required to consider interaction of involved physics and translate this interaction into the form of multi physics coupling. Waste heat energy is provided as an input to the OHP. The piezoelectric patch attached inside the OHP, is displaced under the pressure exerted by the fluid flow oscillating with a certain frequency, which generates the output electrical energy. Such a close interaction in between solid and fluid can be assumed to have a form of a fully coupled model. A fully coupled model will capture the interaction in between thermal physics, fluid flow and solid mechanics. This coupling will be formed in three stages –

1) 1^{st} stage: Thermo-hydrodynamic interaction - Calculate pressure differential based on provided heat input
2) 2^{nd} stage: Fluid-structure interaction - Calculate the fluid velocity based on the pressure differential and form a fluid -solid coupling to calculate stresses developed in the piezoelectric material due to oscillatory fluid flow
3) 3^{rd} stage: Piezoelectric effect - Calculate voltage generated due to piezoelectricity

The following sections discuss governing equations of each of the above mentioned physics and analytical equations used to create a multi physics coupling.

3.2 Oscillating Heat Pipes

3.2.1 Structure and operating principle

An oscillating heat pipe is a heat transportation device in which an elongated metallic capillary tube is formed having an inner diameter sufficiently small to enable movement of a bi-phase compressible working fluid [31]. Closed loop oscillating heat pipe is a long meandering tube with several turns and sealed at both the ends. The tube is evacuated and then partially filled with a working fluid. OHP is heated at the evaporator section and cooled at condenser section. The liquid and vapor then get distributed throughout the pipe as liquid slugs and vapor bubbles. As the evaporator section of the OHP is heated, the vapor pressure of the bubbles located in that section will increase. This forces the fluid towards the condenser section of the heat pipe. When the vapor bubbles reach the condenser section, they begin to condense. As the vapor changes phase, the vapor pressure decreases, and the liquid flows back towards the condenser end. In this way, a steady oscillating flow is set up in an OHP. Heat addition and rejection and growth and extinction of vapor bubbles drive the flow of OHP [35].

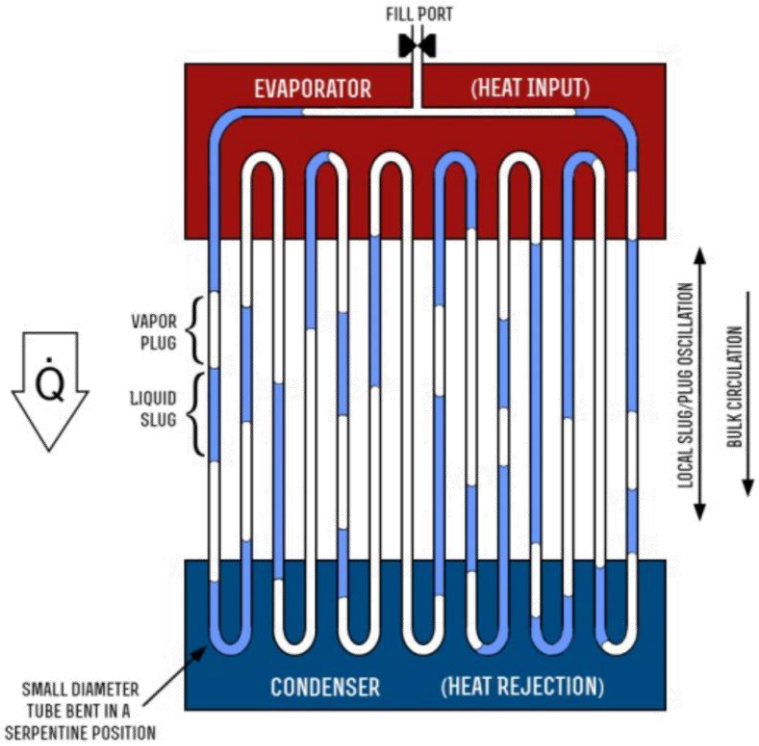

Fig. 3.1: Schematic representation of oscillating heat pipe [36]

3.2.2 Operating parameters and interdependence

For our work, it is important to formulate a relationship in thermal and fluid parameters of the OHP. Closed loop oscillating heat pipes are complex heat transfer systems with a very strong thermo-hydrodynamic coupling governing thermal performance. Different heat inputs gives rise to different flow patterns inside the tubes. OHP performance gets influenced by various operating parameters such as working fluid, internal tube diameter, total tube length, length of the condenser and evaporator sections, number of turns and an inclination angle [37]. Relation between the heat flux and operating parameters can be stated as given in Eq. (1),

$$q = \frac{Q}{\pi . D_i . N . 2L_e} \quad (1)$$

Where, q is the heat flux, Q is the heat input, D_i is the internal diameter of the OHP, N is number of turns and L_e is the effective length of the OHP.

In order to find out the heat transfer correlations having broad applicability range, thermo-physical properties of the heat transfer need to be stated as non-dimensional quantities. A semi empirical relation was formed based on three dimensionless groups, the Karman number (Ka_{liq}), the liquid Prandtl number (Pr_{liq}) and the Jacob Number (Ja). These numbers are used to form a correlation between different operating parameters and the thermal input [38].

$$Ka_{liq} = \frac{\rho_{liq}(\Delta P)_{liq} D_i^2}{\mu_{liq}^2 L_{eff}} \text{ , where, } L_{eff} = 0.5(L_e + L_c) + L_a \quad (2)$$

$$\underset{liq}{\Pr} = \frac{C_{p,liq}\, \mu_{liq}}{k_{liq}} \quad (3)$$

$$Ja = \frac{h_{fg}}{C_{p,liq}\, (\Delta T)^{e-c}{}_{sat}} \quad (4)$$

Where, $\rho_{liq}, \mu_{liq}, C_{p,liq,} h_{fg}$ are density, dynamic viscosity, specific heat and enthalpy of vaporization of the fluid respectively. D_i, L_{eff} is diameter and effective length of the OHP. ΔP and ΔT is the pressure and temperature differential.

Thermo-physical properties are calculated at $(T_e + T_c)/2$ to get an average temperature distribution. The liquid Prandtl number scales the single phase convective effect on heat transfer while the Jacob number highlights the relative importance of sensible and latent

heat portions of heat transfer in a closed loop oscillating heat pipe. An exponential function was added to be represent the effect of inclination angle (β).

Based on experimental measurements, a semi-empirical relationship was formulated [37],

$$q = 0.54(\exp(\beta)^{0.48})Ka^{0.47}Ja^{1.43}N^{-0.27}\mathrm{Pr}_{liq}^{0.27} \quad (5)$$

Based on the heat flux input to the OHP, pressure differential inside the OHP can be calculated by using Eq. (1) and (5). This is an important correlation in between the thermo-hydrodynamic properties of the OHP. However, it must be noted that this relationship was formulated for a specific experimental condition and hence it can't be used to accurately estimate the pressure differential value. This relationship can be used to find an approximate value of a pressure differential which can be used to form a fluid-solid coupling.

3.3 Fluid-Solid Interaction Coupling

Pressure differential inside an OHP is responsible for the generation of oscillatory flow inside the tube. The piezoelectric patch is placed in an adiabatic section inside the OHP tube. Bi-phase fluid oscillating in between the evaporator and condenser section will exert pressure on the piezoelectric patch upon encounter. Fluid-structure interaction is a multi physics coupling between laws describing the fluid dynamics and structural mechanics physics. When a fluid encounters a structure, stresses and strains are exerted on the solid objects that lead to deformations. These deformations can be quite large or very small depending on the pressure and velocity of the flow and material properties of the structure. If the deformations are large, the velocity and pressure fields of the fluid will

change as a result, and such a problem is treated as bidirectionally coupled fluid-structure interaction.

3.3.1 Governing equations for fluid-structure interaction

Navier-Stokes equation provides a solution for velocity field considering fluid flow physics [39]:

$$\rho\left(\frac{\partial u}{\partial t}+u.\nabla u\right)=-\nabla p+\nabla.\left(\mu(\nabla u+(\nabla u)^{T})-\frac{2}{3}\mu(\nabla.u)\right)+F \tag{6}$$

Where, u is the fluid velocity, p is the fluid pressure, ρ is the fluid density, μ is the fluid dynamic viscosity, and F is the external applied force.

Navier-Stokes equations are always solved together with continuity equation:

$$\frac{\partial \rho}{\partial t}+\nabla.(\rho u)=0 \tag{7}$$

The Navier-Stokes equations represent the conservation of momentum, while the continuity equation represents the conservation of mass.

The total force exerted on the solid boundary by the fluid is the negative of the reaction force on the fluid [40].

$$\sigma_{fluid}=-p_{fluid}+\mu\left(\nabla u_{fuid}+\left(\nabla u_{fluid}\right)^{T}\right)-\frac{2}{3}\mu(\nabla.u_{fluid}) \tag{8}$$

In Eq. 8, p denotes the pressure, μ is the dynamic viscosity for the fluid, and n is outward normal to the boundary.

In a closely coupled fluid-structure interaction, it is safe to assume that the velocity of fluid is transferred to the solid at the surface of interaction [40].

$$u_{fluid} = v_{wall} \tag{9}$$

$$v_{wall} = \frac{\partial u_{solid}}{\partial t} \tag{10}$$

$$\sigma_{solid}.n = \sigma_{fluid}.n \tag{11}$$

Stress generated in the piezoelectric material is calculated using Eq. 8,9,10 and 11. Analytical method of calculating electrical potential using the stress value obtained by solving fluid-structure interaction is explained in the next section.

3.4 Piezoelectricity

Piezoelectricity is a form of coupling between the mechanical and the electrical behaviors of ceramic and crystals belonging to certain classes [41]. Discovered in 1880 by Curie brothers, these materials when mechanically strained, produce electric polarization that is proportional to the applied strain, depicting direct piezoelectric effect. In converse piezoelectric effect, when the same material is subjected to an electrical polarization, strain proportional to the polarizing field is created in the material. These two effects coexist in a piezoelectric material. Direct piezoelectric effect is of particular interest in applications like vibration based energy harvesting.

Several natural crystals such as Rochelle salt, quartz, Topaz and some organic substances as silk, wood, enamel etc are observed to be exhibiting the piezoelectric effect.

However, in order to use them in engineering applications, the electromechanical coupling between the mechanical and electrical behaviors of the materials has to be sufficiently strong. Piezoelectric ceramics were developed in the second half of the last century and they exhibit much stronger coupling compared to natural crystals. PZT was developed in Tokyo Institute of Technology in the 1950s and various versions of it gain wide popularity in energy harvesting applications [41].

The standard form of piezoelectric constitutive equations can be given in tensorial representation of strain-electrical displacement form where the independent variables are the stress components and electric field components.

$$S = s_E T + d^t E \tag{12}$$

$$D = dT + \varepsilon_T E \tag{13}$$

Equations (12) and (13) can be written in a matrix form as

$$\begin{bmatrix} S \\ D \end{bmatrix} = \begin{bmatrix} s^E & d^t \\ d & \varepsilon^T \end{bmatrix} \begin{bmatrix} T \\ E \end{bmatrix} \tag{14}$$

Where, the superscripts E and T denote that the respective constants are evaluated at constant electric field and constant stress, respectively, and superscript t stands for the transpose. S is the strain, T is the stress, E is the electric field, D is the electric displacement field, s^E is the compliance matrix, ε^T is the dielectric matrix evaluated at constant mechanical stress, and d is the piezoelectric coupling matrix [41].

Some important parameters that determine performance of a piezoelectric material are summarized below [42].

Coupling Factor (k_{ij}): The coupling factor k_{eff} is a measure of the effectiveness with which electrical energy is converted into mechanical energy and vice versa.

$$k_{eff}^2 = \frac{\text{energy converted}}{input\ energy} \tag{15}$$

Permittivity (ε_{ij}): The absolute permittivity is defined as the dielectric displacement per unit electric field. The first subscript gives the direction of the dielectric displacement, the second gives the direction of the electric field.

Compliance (s_{ij}): The compliance of a material is defined as the strain produced per unit stress. The first subscript refers to the direction of the strain, the second to the direction of the stress.

3.5 Electrostatics

Under static conditions, the electric potential, V, is defined by the relationship:

$$E = -\nabla V \tag{16}$$

Combining Eq.15 with constitutive relationship $D = dT + \varepsilon_T E$ between the electric displacement (D) and the electric field (E), it is possible to solve the Gauss's law to find the value of electric potential.

CHAPTER FOUR

EXPERIMENTAL APPROACH

In this research, experiments were conducted to measure the voltage produced by the energy harvesting apparatus. Voltage data recorded by experiments for different heat input conditions has been compared with voltage estimated by the numerical model developed in this work. These experiments were conducted in collaboration with Dr. Scott Thompson of Auburn University.

4.1 Experimental Setup

A 4-turn tubular OHP was fabricated from copper tubing with an internal diameter of 5mm. This diameter value was decided based on the condition of Bond number. A section of square brass tubing with 3.25 mm side was used as a harvesting module. Two openings were cut into one side of the square tube to allow the piezoelectric patch to form a bow spring inside the tube. A viewing port was added to the square harvester pipe to observe the fluid as it oscillated around the piezoelectric patch. Macro fiber composite (MFC) piezoelectric transducer from Smart Material (M-8503-P2) was used for the purpose of energy harvesting. The length of the patch was 8mm x 113 mm and was coated with an environmental coating. The leads for the circuit connections were on opposite ends of the transducer, kept outside the square tubing for the ease of electrical connections. This assembly of the harvester module was then installed in-line with a tube in the adiabatic section of the OHP. A two-part epoxy adhesive was used to seal the connection with round tubes, the openings for the piezoelectric path, and the viewing polycarbonate window [43].

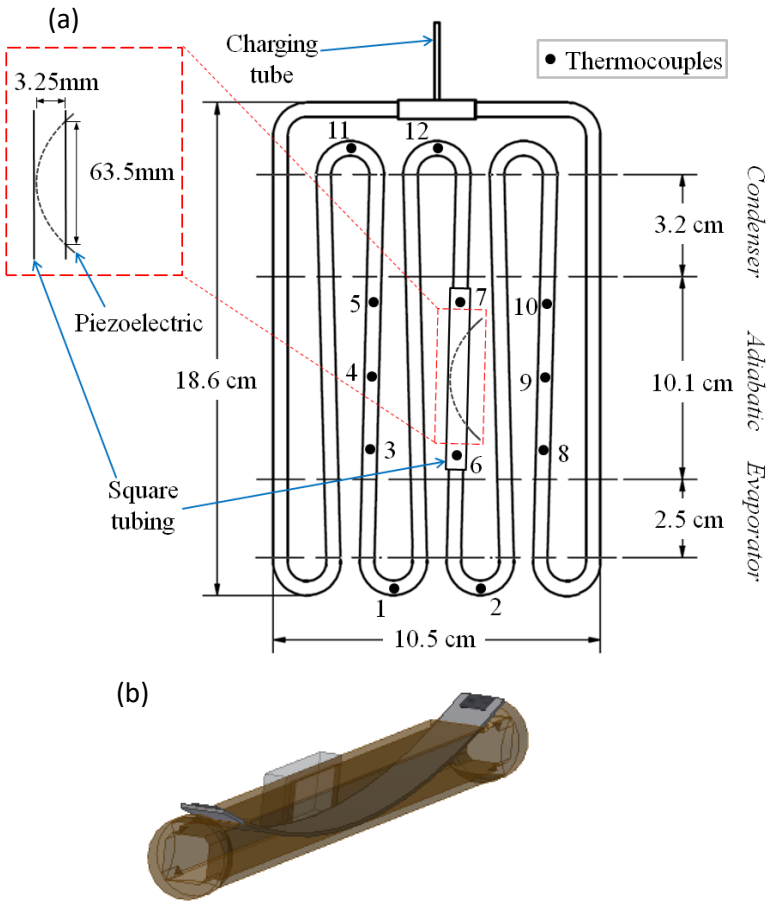

Fig. 4.1 a) OHP configuration 2) Harvesting module [43]

Twelve thermocouples were affixed to the outside wall to record the temperature at various locations. The OHP was evacuated and then filled with water as a working fluid with a filling ratio of ~80%. The charging tube was then hermetically sealed. Water at 15° C was circulated through the aluminum water blocks around the condenser section of the OHP. Two 10cm, 300W cartridge heaters were controlled by a Variac to provide thermal input to heater blocks around evaporator section. The OHP test assembly was well insulated, and the OHP thermal performance calculations assume that all the electrical

power input is transferred through the OHP as heat until it is removed from the assembly at the water blocks.

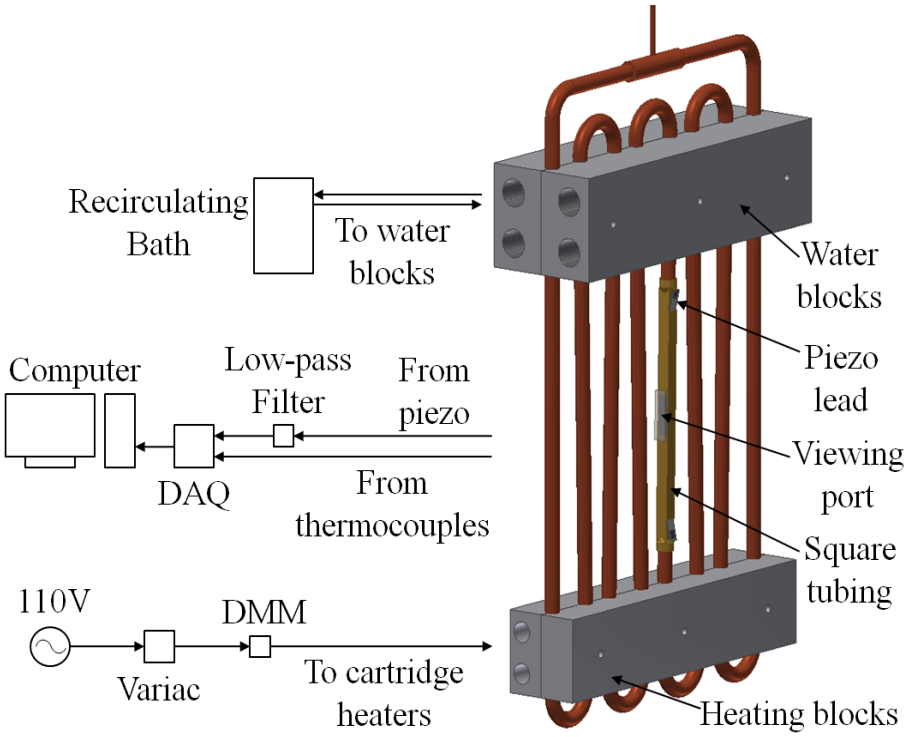

Fig. 4.2 OHP Test Assembly

A National Instruments data acquisition (DAQ) system collected temperature and voltage data. Tests were conducted at 10 to 50W and then increased by 50W increments until maximum temperature oscillation spikes reached 100° C. Testing concluded at 100° C to reduce the chance of seal failure. Temperature and voltage data was collected for two minutes at higher heat inputs.

4.2 Experimental Results

4.2.1 Thermal parameters

Effective thermal conductivity across the OHP adiabatic region was calculated using Fourier's law. The effective thermal conductivities for the OHP with and without the piezoelectric are shown in Fig. 4.3

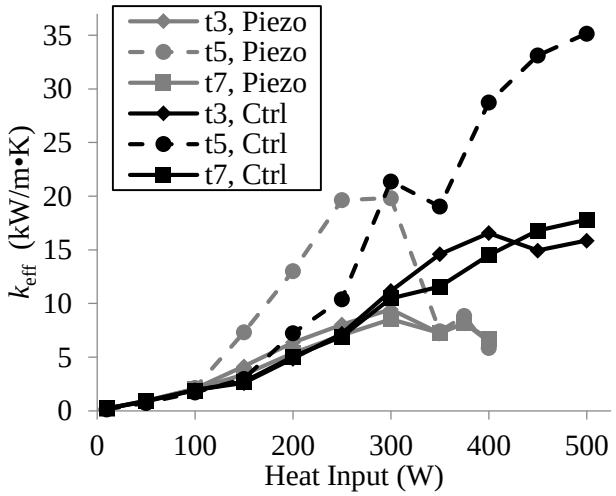

Fig. 4.1. Effective thermal conductivity vs. heat input for round tubes (t3 and t7) and square tube (t5) with and without the piezoelectric.

4.2.2 Fluid Parameters

The polycarbonate viewing window allows direct visualization of the OHP working fluid, which was filmed at 120 fps at each heat input. The fluid oscillations are supposed to have occurred at 1-4Hz [43]. Due to charging ratio of ~80%, and limitations posed due to location of the viewing port, much of the liquid seen through the window was in liquid phase and hence couldn't be tracked. However, location of visible liquid-vapor interface

was manually tracked to calculate average fluid velocity as shown in Fig.4. These values are recorded without a piezoelectric patch attached inside the OHP and hence only considers control OHP's behavior.

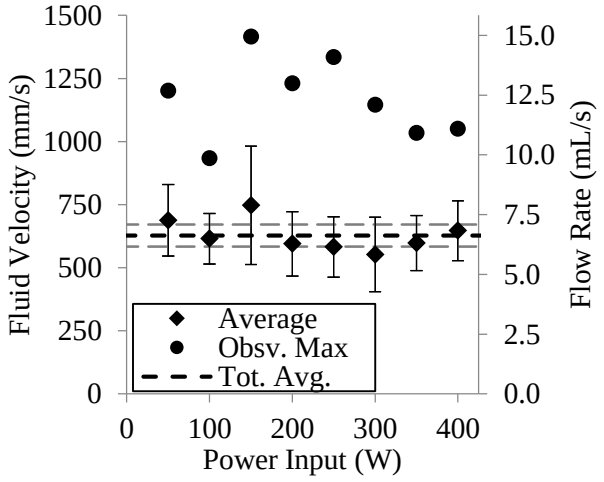

Fig. 4.4. Fluid velocity vs heat input for control OHP

As seen from Fig. 4.4, average fluid velocity recorded was 628±44 mm/s (average flow rate is 6.63±0.46 mL/s). A separate liquid manometer experiment was conducted to calculate pressure drop due to piezoelectric patch across the adiabatic section. The pressure drop couldn't be recorded during OHP operation. Pressure drop was recorded for various flow rate values are shown in fig.4.5

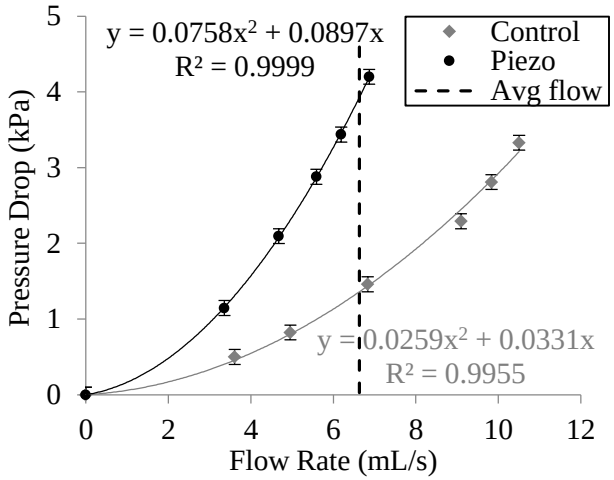

Fig. 4.5. Pressure drop vs flow rate with and without piezoelectric patch

4.2.3 Energy Harvesting

The maximum peak-to-peak open circuit voltage produced by the OHP was 63mV at 400 W heat input. A general decrease in voltage generation was seen between 100-300 W heat inputs. VOC signal recorded for 150 W heat input is shown in Fig. 4.6.

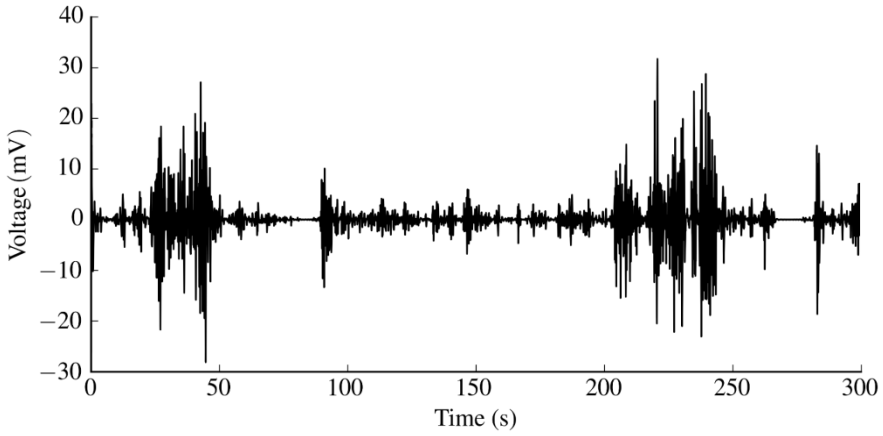

Fig. 4.6. VOC vs time at 150 W heat input

CHAPTER FIVE

THERMO-HYDRODYNAMIC INTERACTION

5.1 Numerical Approach for Thermo-Hydrodynamic Interaction

To develop a numerical model of energy harvesting, it is crucial to replicate the operation of OHP to understand behavior and effect of oscillating fluid on the deformation of piezoelectric patch and electric potential. For this work, it is necessary to create thermo-fluid-structure-electrostatics coupling in the numerical model. However, due to data limitation, it is not possible to integrate thermo-hydrodynamic coupling with fluid-structure coupling. Hence, an independent analysis was done to replicate thermo-hydrodynamic coupling and generate output fluid parameters based on input oscillating heat pipe operating conditions. Fluid pressure differential needed to develop an oscillatory flow structure inside the OHP is an important parameter. Using the value of pressure differential, it is possible to accommodate the effect of thermo-hydrodynamic coupling to construct the multi-physics coupling in between fluid-structure-electrostatic physics.

Vapor pressure difference between the two vapor plugs at two end of the liquid slug is responsible for generation of oscillatory flow. This vapor pressure difference is given by eq. 17,

$$P_i - P_{i+1} = A_i cos\omega_i t \tag{17}$$

However, the amplitude and angular frequency are unknown a priory as the pressure difference depends on heat transfer in two vapor plugs. Zhang and et al proposed

a numerical investigation method which can be used to analyze the oscillatory flow in OHP [44][45]. In this method, the governing equations are first non-dimensionalized and the parameters of the system were reduced to dimensionless numbers. The non-dimensional governing equation are then solved numerically and the effects of various parameters on an oscillatory flow of the OHP are investigated [46]. Using this numerical investigation, it is possible to predict the amplitude of the pressure difference *a priori*.

5.1.1 Model Description

The model under consideration consists of n number of turns with diameter d and length 2nL. The evaporator sections of the OHP are at the upper portion and each of them has a length of $L_{h..}$ The condenser section is located in the lower portion of the OHP with length L_c and adiabatic section has a length of L_a. The wall temperature at the evaporator and condenser sections are T_e and T_c respectively. The liquids slugs with uniform length of $2L_p$ are located in every tube, entrapping vapor plug between two liquid slugs. The location of each liquid slug is represented by x_i which is positive when the liquid slug moves right, negative when it moves back to the left, and zero when the liquid slug is exactly in the middle.

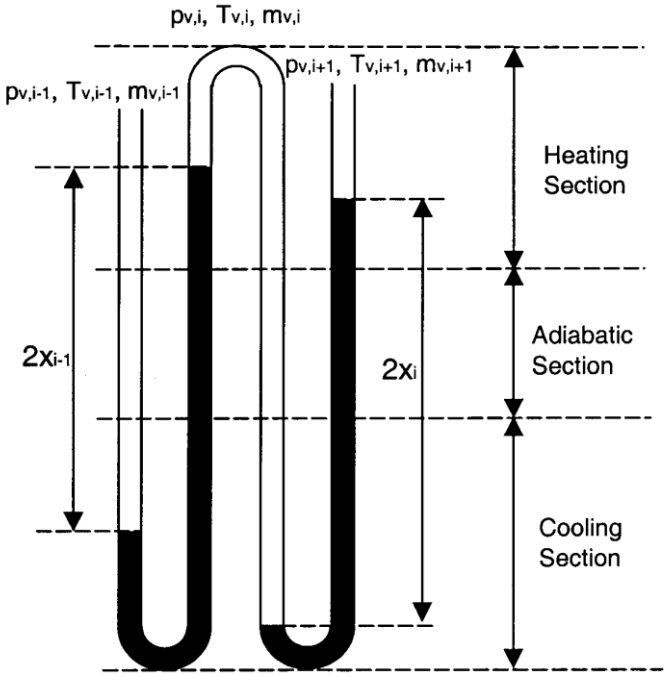

Fig. 5.1 Schematic description of OHP model

5.1.2 Governing equations

The momentum equation for the liquid slug is given by,

$$2A_c L_p \rho_l \frac{d^2 x_i}{dt^2} = \left(p_{v,i} - p_{v,i+1}\right)A_c - 2\rho_l g A_c x_i - 2\pi d L_p \tau_p \tag{18}$$

Eq. 18 is rewritten as,

$$\frac{d^2 x_i}{dt^2} + \frac{32\vartheta_e}{d^2}\frac{dx_i}{dt} + \frac{g}{L_p}x_i = \frac{p_{v,i} - p_{v,i+1}}{2\rho_l L_p} \tag{19}$$

The energy equation of the vapor plugs is obtained by applying the first law of thermodynamics to each plug,

$$\frac{d\left(m_{v,i}c_vT_{v,i}\right)}{dt} = c_pT_{v,i}\frac{dm_{v,i}}{dt} - p_v\frac{\pi d^2}{4}\left(\frac{dx_i}{dt} - \frac{dx_{i-1}}{dt}\right) \tag{20}$$

Using ideal gas law, behavior of vapor plugs in the evaporators is modeled as,

$$p_{v,i}\left[2\left(L - L_p\right) + x_i - x_{i-1}\right]\frac{\pi d^2}{4} = m_{v,i}R_gT_{v,i}, \quad i = 1,2,3,..,n \tag{21}$$

A closed form of the mass of vapor plugs is obtained as,

$$m_{v,i} = C_iT_{v,i}^{\frac{1}{\gamma-1}}\left[2\left(L - L_p\right) + x_i - x_{i-1}\right], \quad i = 2,3,\dots,n \tag{22}$$

Masses of vapor plugs increase due to evaporation and decrease due to condensation

$$\frac{dm_{v,i}}{dt} = \frac{h_e\pi d\left(T_e - T_{v,i}\right)\left(L_{h,L} + L_{h,R}\right)}{h_{fg}} - \frac{h_c\pi d\left(T_{v,i} - T_c\right)\left(L_{c,L} + L_{c,R}\right)}{h_{fg}} \tag{23}$$

Where, $L_{h,L}$ and $L_{h,R}$ are lengths of evaporator sections in contact with the vapor plug and $L_{c,L}$ and $L_{c,R}$ are lengths of condenser sections in contact with the vapor plug.

5.1.3 Non-dimensional governing equations

Considering a reference state of OHP with pressure, displacement and temperature as $p_{0,}$ $x_i=x_0$ and T_0 respectively.

Let us define dimensionless quantities as,

$$\theta_i = \frac{T_{v,i}}{T_0}, \quad P_i = \frac{P_{v,i}}{P0}, \qquad M_i = \frac{m_{v,i}}{m_0}, \qquad X_i = \frac{x_i}{x_0}, \varepsilon = \frac{L_p}{L}, \tag{24}$$

$$\tau = \frac{\vartheta t}{d^2}, \omega^2 = \frac{g d^4}{L_P \vartheta}, \zeta = \frac{p_0 d^4}{2\rho_l L_p L_h \vartheta^2}$$

Where, θ_i, P_i, M_i, $X_{i,}$ ε, and τ are dimensionless temperature, pressure, mass of the vapor plug, liquid slug displacement, charge ratio, and time respectively. ω is the dimensionless inherent angle frequency and ζ is the dimensionless parameter during the non-dimensional process.

Substituting eq. 23 in eq. 18 and eq. 22, we obtain,

$$\frac{d^2 X_i}{d\tau^2} + 32\frac{dX_i}{d\tau} + \omega^2 X_i = \zeta(P_i - P_{i+1}) \tag{25}$$

$$\frac{dM_i}{d\tau} = H_e\left(L^*_{h,L} + L^*_{h,R}\right)(\theta_e - \theta_i) - H_c(L^*_{c,L} + L^*_{c,R})(\theta_i - \theta_c) \tag{26}$$

Where,

$$H_c = \frac{4h_c RT_0^2 d}{p_0 h_{fg} \vartheta_e}, \qquad H_e = \frac{4h_e RT_0^2 d}{p_0 h_{fg} \vartheta_e}, \qquad \theta_c = \frac{T_c}{T_0}, \quad \theta_e = \frac{T_e}{T_0} \tag{27}$$

$$M_1 = \theta_1^{\frac{1}{\gamma-1}} \left[\frac{1}{2} + \frac{X_1}{2(1-\varepsilon)}\right] \tag{28}$$

$$M_i = \theta_i^{\frac{1}{\gamma-1}} \left[1 + \frac{X_i - X_{i-1}}{2(1-\varepsilon)}\right], \qquad i = 2,3,..,n \tag{29}$$

$$M_{n+1} = \theta_{n+1}^{\frac{1}{\gamma-1}} \left[\frac{1}{2} - \frac{X_n}{2(1-\varepsilon)}\right] \tag{30}$$

$$P_i = \theta_i^{\frac{\gamma}{\gamma-1}} \tag{31}$$

5.1.4 Initial Conditions

$$X_i = X_0, \qquad \tau = 0, \quad i = 1,2,\dots,n \tag{32}$$

$$\theta_i = 1, \qquad \tau = 0, \qquad i = 1,2,\dots,n \tag{33}$$

$$M_1 = \frac{1}{2} + \frac{X_0}{2(1-\varepsilon)}, \qquad \tau = 0 \tag{34}$$

$$M_i = 1, \tau = 0, \qquad i = 2,3,..,n \tag{35}$$

$$M_{n+1} = \frac{1}{2} - \frac{X_0}{2(1-\varepsilon)}, \qquad \tau = 0 \tag{36}$$

5.1.5 Numerical Analysis Setup

The amplitude and angular frequency of pressure oscillation is unknown. To find these parameters, dimensionless governing equations are solved for each time step using an implicit scheme [47]. The numerical procedure followed in this approach is outlines as follows-

1) Guess the dimensionless temperature of all vapor plugs, θ_i
2) Use eq. 31 to obtain dimensionless pressure, P_i
3) Use eq. 25 to calculate dimensionless displacement of liquid slug, X_i
4) Use eq. 26 to calculate mass of vapor plugs
5) Use eq. 28,29,30 to calculate dimensionless temperature of the vapor plugs, θ_i
6) Compare θ_i obtained in 1st and 5th step, and if the tolerance meets the desired value repeat this procedure for next time step, else repeat this process by setting the guess value of θ_i in 1st step with the value of θ_i obtained in 5th step.

5.1.5 Results and Discussion

A MATLAB code was developed to solve the numerical analysis outlined in 5.1.6. For the n-turn OHP, there are (n+1) vapor plugs and n liquid slugs. To obtain a time step independent solution, time step of $\Delta\tau=10^{-5}$ was selected [46]. Dimensionless parameters used in this analysis were obtained by input parameters including number of turns, geometric parameters of the OHP, fill ratio, temperature of condenser and evaporator section, initial pressure and temperature, and thermal properties of water.

Pressure magnitude for the 2nd and 3rd vapor plug represent the vapor plugs in 2nd and 3rd OHP turn respectively. Using numerical analysis procedure listed in earlier sections, pressure difference responsible for the oscillatory flow in the 3rd turn can be calculated by calculating vapor plug pressure. Using the value of pressure difference, it is possible to calculate the value of the magnitude of pressure difference.

Dimensionless pressure versus time behavior for vapor plug 2 and 3 can be seen in fig 5.2 and fig. 5.3,

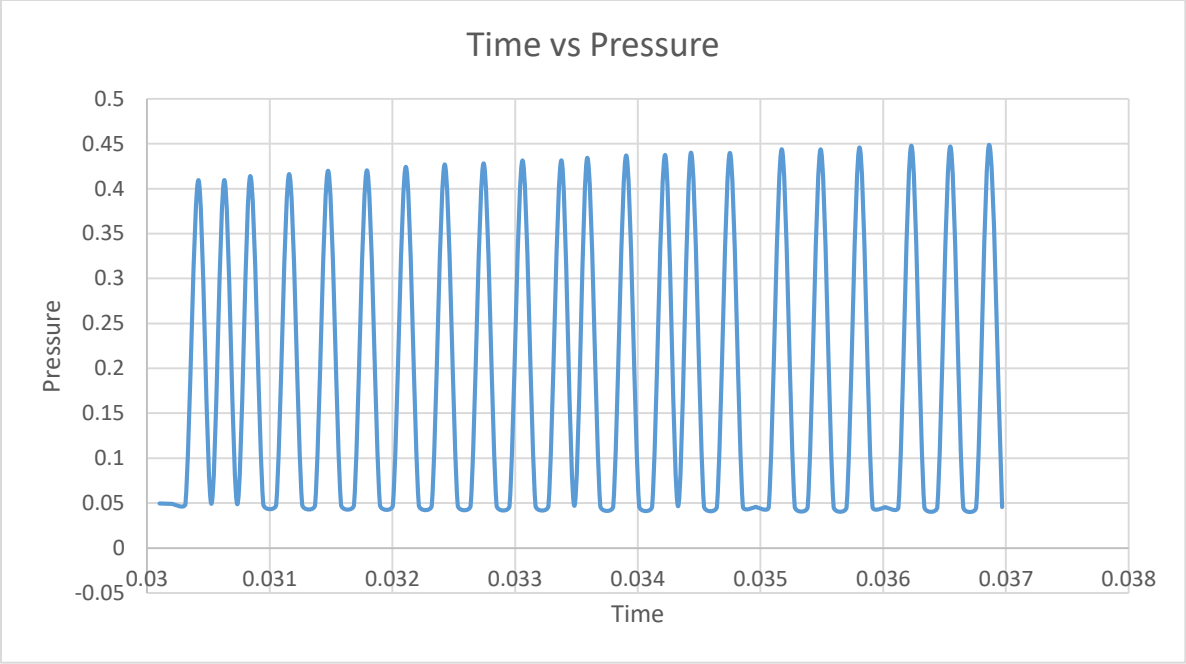

Fig. 5.2 Pressure vs time behavior of 2nd vapor plug

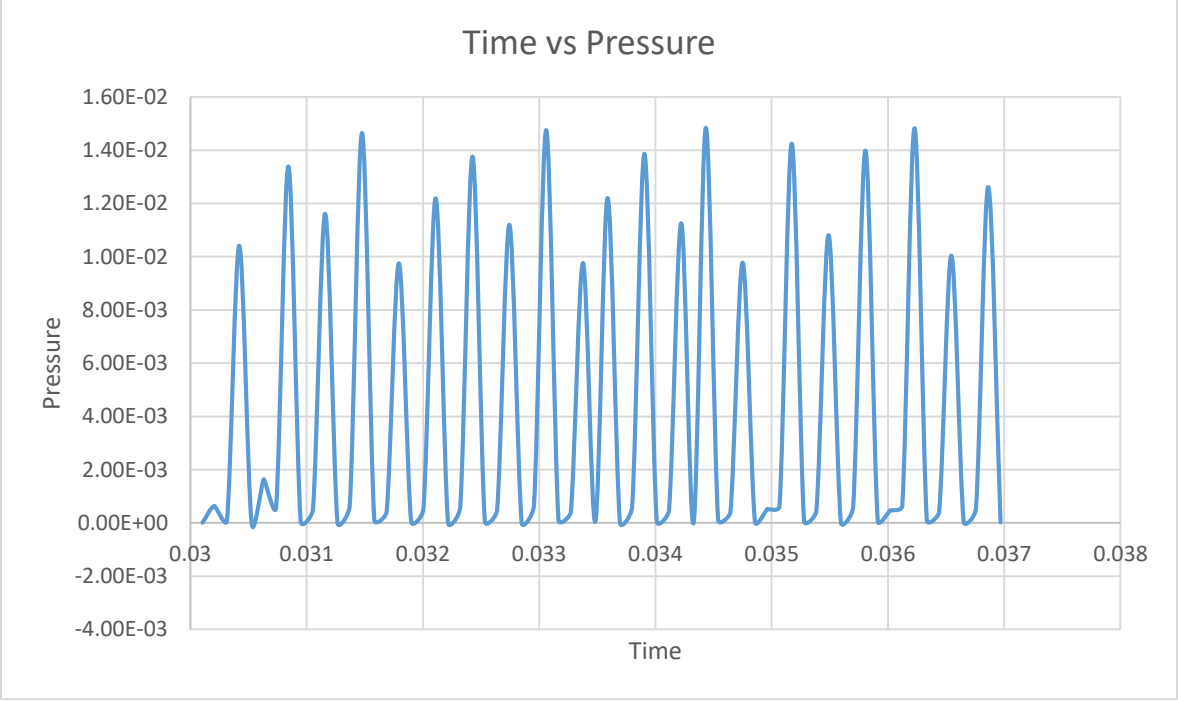

Fig 5.3 Pressure vs time behavior of 3rd vapor plug

Pressure values can be observed to depict a sinusoidal waveform varying with respect to time. By using eq. 24, dimensional vapor pressure for 2nd and 3rd vapor plug can be calculated for a particular time instant. These values are then used to calculate magnitude of the pressure difference. Pressure differential value obtained by developed numerical procedure shows consistent results with analytical procedure explained in section 2.2.2. Pressure differential value is used as an inlet boundary condition in the laminar flow physics described in the next chapter.

Table 5.1 Comparison of results using different approaches

Approach	Value of pressure differential
Analytical	1122 Pa
Numerical using MATLAB	1030 Pa

The main advantage offered by the numerical procedure is the ability to produce *a priori* results of a complex thermo-hydrodynamic phenomenon. This method can provide pressure differential value for varying value of heat inputs, number of turns, fill ratio, working fluid, and angle of inclination of the OHP.

CHAPTER SIX

NUMERICAL ANALYSIS AND COMPARISON OF RESULTS

This chapter will discuss the numerical analysis approach and details of finite element simulations. Results obtained from 3D numerical analysis are compared with experimentally recorded results and reasons for variations are discussed latter in the chapter.

6.1 Finite Element Analysis with Multi-physics Coupling

Finite element analysis models are built as predictive computational models of real-world scenarios. A reliable and accurate numerical model is very useful in analyzing the behavior of the system, thereby eliminating the need of costly experimentations. However, it is important to consider the cost of computational time and memory requirements associated with finite element modeling. A good starting point of approaching this issue is to check if 2D simulations is a viable solution. A 2D analysis provides quicker results at the cost of relatively lesser memory requirement, allowing for design iterations in the same time as time required for a 3D analysis. Also, in a highly nonlinear problem, observations from 2D analysis can help in convergence efficiency of future 3D runs. A multi-physics coupled analysis is computationally expensive. Hence, it was decided to build a 2D numerical analysis model to get better understanding of nature of problem by allowing multiple iterations exploring different approaches. COMSOL multi physics FEA software was used for the development of the numerical model. Simulation set up and results of the 2D analysis are explained in appendix A.

Results obtained from 2D analysis are not accurate due to limitations in building the exact geometry. Another important reason of developing a 3D numerical analysis model is to get rid of division of fluid domain as shown in fig. 6.1.

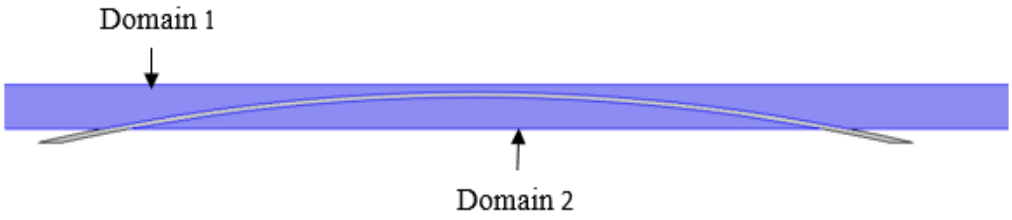

Fig. 6.1 Enlarged view of fluid domain in 2D model

In a 2D numerical model, fluid domain depicting the flow inside the OHP pipe gets divided in two domains-upper domain and lower domain. This is caused by the presence of piezoelectric patch separating the fluid flow in 2D model. Due to the separation of the flow, force condition assigned at the inlet can't drive the flow present under the piezoelectric patch and hence the fluid present under the patch doesn't exhibit oscillatory motion. Fluid displacement in the domain 2 is observed simply due to the displacement of piezoelectric patch. To overcome this limitation, it is necessary to develop a 3D numerical model with 3D CAD geometry. In a 3D geometry, fluid domain isn't separated and hence the water flow around the piezoelectric patch is driven by the same pressure condition at the inlet.

In the experimental setup, the harvester module was affixed on one of the four turns of the oscillating heat pipe. Due to limitation of data availability, for the purpose of this thesis, it is sufficient to consider only harvester module in isolation without constructing

an oscillating heat pipe assembly. Pressure differential boundary condition is evaluated considering thermo-hydrodynamic coupling as discussed in Ch. 5 and appropriately assigned in the analysis.

6.2 3D Numerical Analysis Setup

6.2.1 Geometry

The harvester module geometry was designed as a rectangular pipe with a piezoelectric patch attached inside it. Length of the rectangular pipe is kept equivalent to entrance length to allow fully developed laminar flow. The piezoelectric patch's ends were modelled to extrude from the pipe to facilitate electrical circuit connection.

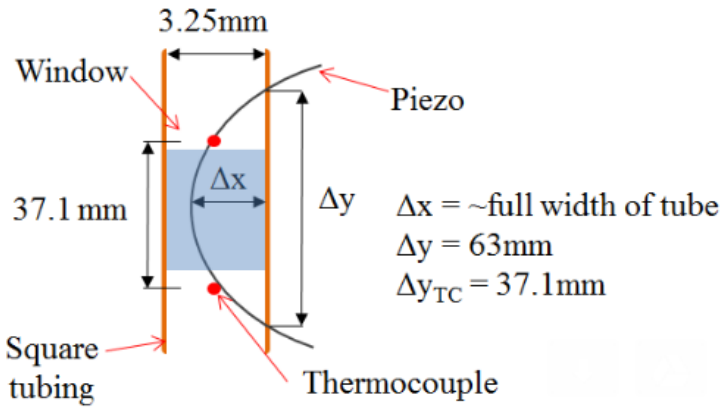

Fig. 6.2. Energy harvester assembly dimensions

3D simulation is done by building a 3D symmetric numerical model. As the geometry under consideration is symmetric, only half of the geometry can be analyzed. Obtained results are then appropriately post processed to analyze the effect on an entire geometry. This is an effective method of reducing the overall computation time. In 3D

CAD model, the piezoelectric patch doesn't occupy the entire pipe width, leaving a little gap on both sides for the fluid to flow under it.

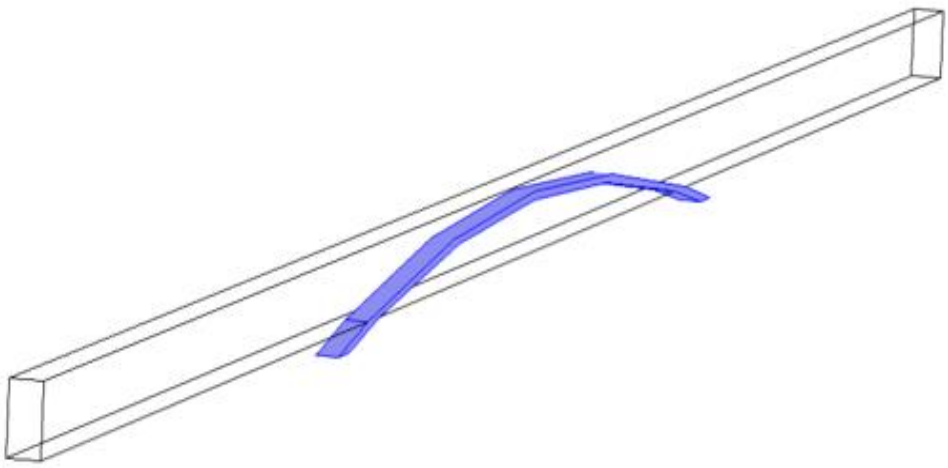

Fig. 6.3. 3D Geometry of harvester module

Table 6.1. Geometric Details

Part	Parameter	Value (m)
Harvester pipe	Length	18e-2
	Height	3.25e-3
	Width	3.25e-3
Piezoelectric patch	Thickness	0.38e-3
	Length	63e-3

6.2.2 Materials

Properties of water are assigned to the rectangular pipe consisting of fluid domain. Macro fiber composite material properties are assigned to the piezoelectric patch. Macro fiber composite was originally developed at NASA's Langley Research Center for aerospace applications. The MFC consists of rectangular piezoelectric ceramic rods sandwiched between layers of adhesive and polyamide film [48]. MFC actuators offer an added advantage as low frequency transducers which makes them a popular choice for energy harvesting purpose. PZT-5A represents the functional part of the MFC actuator [49].

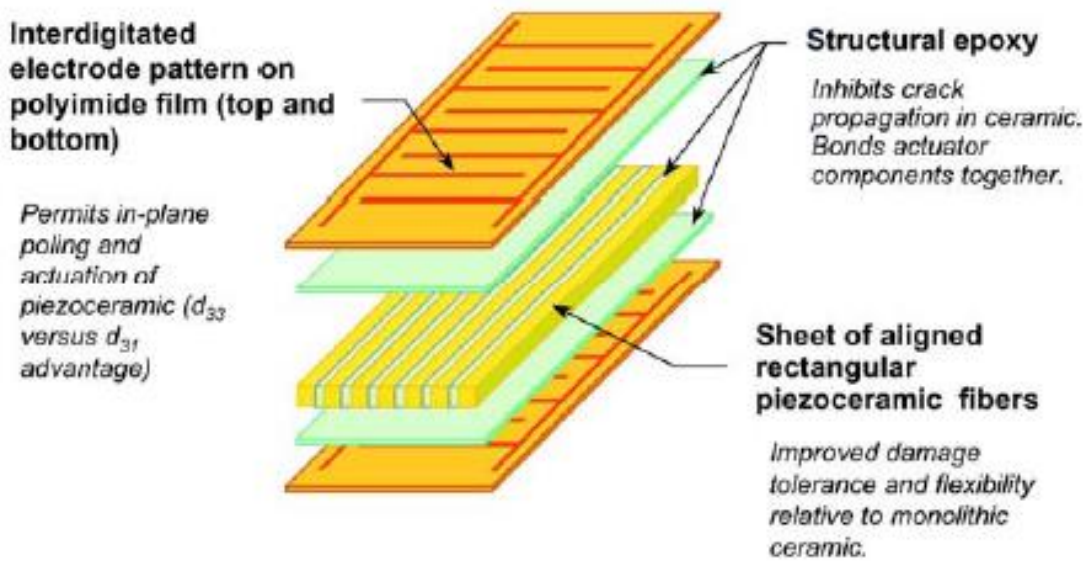

Fig. 6.4 Structure of MFC [48]

Table 6.2 Mechanical parameters of MFC

Material Parameter	Value
Young's modulus	30.33e6 Pa
Poisson's ratio	0.31
Density	5440 kg/m^3

Table 6.3 Material parameters of PZT-5A [49]

Material parameter	Value	Unit
Elastic compliance $s_{11}=s_{22}$	16.4	1e-12 m^2/N
s_{33}	18.8	
$s_{13}=s_{23}$	-7.22	
s_{12}	-5.74	
$s_{44}=s_{55}$	47.5	
s_{66}	44.3	
Piezoelectric coefficient $d_{15}=d_{24}$	584	1e-12 C/N
$d_{31}=d_{32}$	-171	
d_{33}	374	
Relative permittivity $\epsilon_{11}=\epsilon_{22}$	1730	8.854e-12 F/m
ϵ_{33}	1700	
Dielectric loss factor	0.02	-
Mechanical quality factor	60	-

6.2.3 Analysis of the physics

6.2.3.1 Involved Physics

A) Fluid Flow –The flow pattern in OHP falls into three main category- bubbly flow, slug flow, and annular flow [50]. To depict this flow in the numerical model, it is essential to use multi-phase flow modeling techniques as the flow contains liquid and vapor phase of water. However, in this work, the fluid domain under investigation focuses on the fluid flow in the adiabatic region of the OHP where the piezoelectric patch is attached. It has seen experimentally, that the area around piezoelectric consists of water predominantly in liquid phase. Hence, it is safe to assume for the fluid to have a single phase nature for the purpose of this work.

   The oscillatory flow under investigation has a Reynolds's number of 2100, making the flow regime to fall in the transient category. Due to resource limitations, fluid flow is modelled using laminar flow physics in this work.

   Laminar flow physics is used to compute the velocity and pressure fields for a fluid flow in the laminar flow regime. The equations involved in solving laminar flow physics are Navier-Stokes equations for conservation of momentum and the continuity equation for conservation of mass as given by eq. 6 and 7. As water is a Newtonian fluid, eq. 6 and 7 can be closed by using Stokes' assumption to derive viscous stress.

- Boundary Conditions:

No slip boundary condition - No slip boundary condition is assigned on the pipe wall.

Pressure boundary condition – To perform the function of oscillatory flow inside the OHP, it is important to understand the crucial role of boundary condition in the numerical model. Pressure differential as discussed in eq. 17 is responsible to generate the fluid flow of oscillatory nature inside the OHP. It is given as,

$$P_i - P_{i+1} = A_i cos\omega_i t \tag{37}$$

In eq. 37, $P_i - P_{i+1}$ is the pressure difference of two vapor plugs which acts as a driving force for the oscillatory flow. Ai is the amplitude of pressure differential and ω_i is the frequency of oscillation, both of which are unknown *a priori*. Pressure differential is a time dependent cos function which changes its sign for every half cycle. During the first half cycle, the fluid flows in the forward direction. Fluid flow reverses its direction as the pressure differential becomes negative during the second half of the cycle. The procedure of finding the value of A_i is discussed in chapter 5. For our work, the amplitude of pressure differential was found to be 1200 Pa and frequency of oscillation was ~3Hz. Outlet pressure is maintained at 0 Pa.

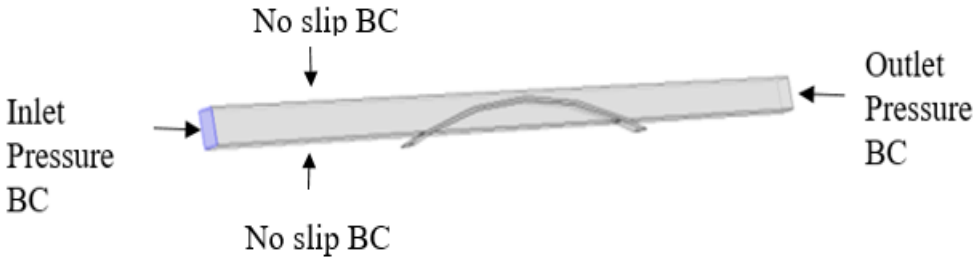

Fig. 6.5 Schematic representation of model set up with boundary conditions

B) Solid Mechanics – The most desirable output of laminar flow physics used to analyze the fluid flow is the value of fluid pressure exerted on the piezoelectric material. In a fluid-structure interaction problem, fluid pressure exerted on the surface of solid results in the solid deformation. Velocity of fluid is equal to velocity of solid which is used in calculation of the piezoelectric patch stress. The stress generated in a piezoelectric material is calculated using eq. 38.

$$\rho \frac{\partial u^2}{\partial t^2} = \nabla . S + F_v \tag{38}$$

- Boundary Conditions:

Fixed Constraint- A fixed point constraint is placed on the intersecting points of the piezoelectric patch. This constraint is used to replicate the fixed ends of the patch in experimental condition. As you can see in fig. 6.6, four fixed point constraints are placed where the piezoelectric patch touches the pipe.

Fig. 6.6 Fixed point constraint in solid mechanics

- Piezoelectric damping:

  Viscous damping: Damping is a material property, important to vibration control. For the mechanical damping treatment of the structure, three parameters are very important, namely, damping, mass and stiffness. Viscous damping, structural damping, and friction damping are a few different types of damping. Viscous damping occurs in piezoelectric transducers at low kHz range. Therefore, it is used in our work.

  When mechanical system oscillates in a fluid medium, such as air, gas, or water, the fluid resistance to body movement causes energy dissipation. It depends on body shape, fluid viscosity, frequency of vibration, etc [51]. The damping forces are expressed as given in eq.39,

$$F = c\dot{u} \tag{39}$$

  Where, c is the constant of proportionality and $\dot{u}$ is the body velocity.

The Raleigh equation is the most widely used way to describe the damping coefficient as given eq. 40,

$$c = \alpha m + \beta k \tag{40}$$

Where, α is the mass multiplication factor and β is the stiffness multiplication factor.

Normally in piezoelectric transducer vibrations, viscous damping is observed. Thus, α=0 and the value of β is calculated as given in eq. 41, which is found to be 0.011 in our case.

$$\beta = \frac{1}{\omega Q_m} \tag{41}$$

Where, Qm is the mechanical quality factor, determined experimentally.

Dielectric loss: Losses in piezoelectric materials can be generated both mechanically and electrically Hysteretic loss corresponds to the phase lag in between the stress and the strain. These losses can be added to the numerical model by several ways- mechanical damping, coupling loss, dielectric loss, etc [52].

All the parameters listed in linear equations of piezoelectricity as given in eq. (12) and (13) must be described by complex numbers, z, and their corresponding loss tangent is defined as [53],

$$\tan \delta_z = \frac{Im(z)}{Re(z)} \tag{42}$$

The imaginary parts of the elastic compliance and dielectric permittivity represent the mechanical and electrical losses. The effect of loss factor in this case is negligible due to low frequency of oscillation. Value of dielectric loss factor used in our work as given by the manufacturer's catalogue is tanδ=0.02 [54].

C) Electrostatics physics – Piezoelectric material defined in solid mechanics physics consists of piezoelectric material properties in strain-charge. Charge conservation principle $E = -\nabla V$ in the electrostatics physics is used to find electrical potential generated by the system.

- Boundary conditions: Electrical boundary conditions are assigned to the two ends of the piezoelectric patch as shown in fig. 6.7

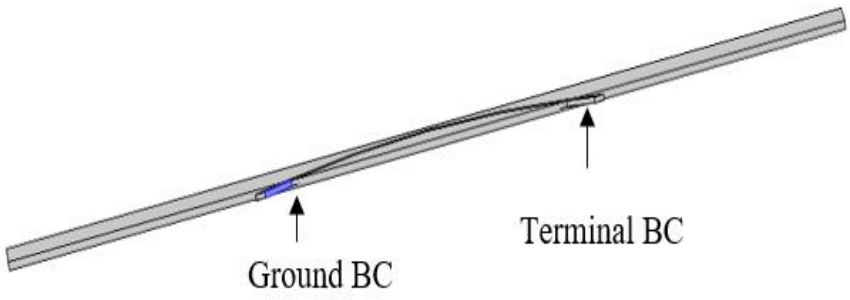

Fig. 6.7 Electrical boundary conditions in electrostatics physics

6.2.3.2 Multi-Physics Coupling

In this numerical model, two multi-physics couplings are created. A fully coupled fluid-structure interaction coupling is used to couple laminar flow physics with solid mechanics. Through this coupling, fluid pressure is used as a loading condition in solid mechanics.

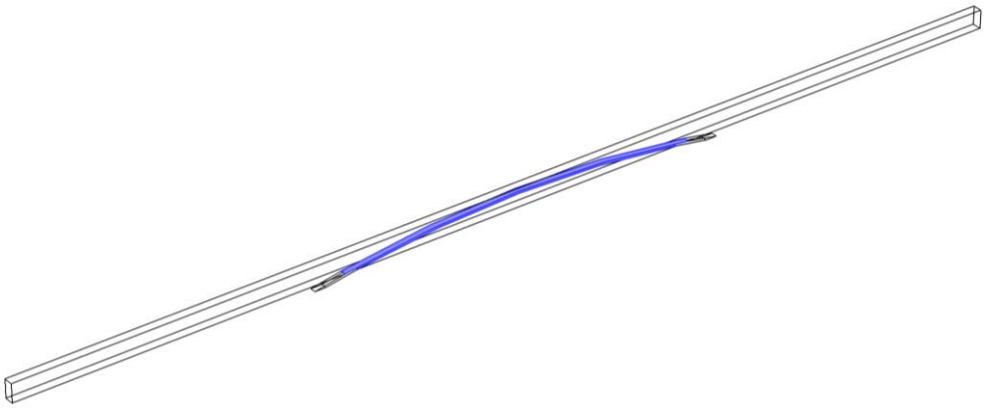

Fig. 6.8 Selection of the boundaries for fluid-structure interaction

Piezoelectric effect coupling is used to couple solid mechanics with electrostatics physics. With this coupling, appropriate relative permittivity from the piezoelectric material defined in solid mechanics is passed on to the charge conservation node in electrostatics.

6.2.4 Mesh

The accuracy of FEA models is directly related to the finite element mesh that is used. The finite element mesh subdivides the CAD model into smaller domains called elements, over which a set of equations are solved. As these mesh elements are refined, the

computed solution will approach the true solution. However, a trade-off needs to be done considering the expensive computational time taken by really fine mesh.

In this work, the numerical model needs to accommodate needs of all the physics involved. A mesh convergence study was carried out to finalize optimal mesh parameters. In 3D numerical model, fluid domain was discretized into coarser tetrahedral elements, whereas the piezoelectric patch was discretized using finer tetrahedral elements. The region of fluid-solid interaction is identified as it needs more attention. Local mesh refinement was done in this area. The entire mesh was calibrated for fluid dynamics application. Three boundary layers were added in the fluid domain along the pipe wall and surface of the piezoelectric patch in contact with the fluid. This type of mesh is needed to resolve the thin boundary layers along the no-slip boundaries. Corner refinement was done to refine mesh structure at sharp corners. Due to bow-like structure of the piezoelectric patch, mesh refinement is necessary to accurately capture the results. Finalized mesh structure consists of 782,199 domain elements.

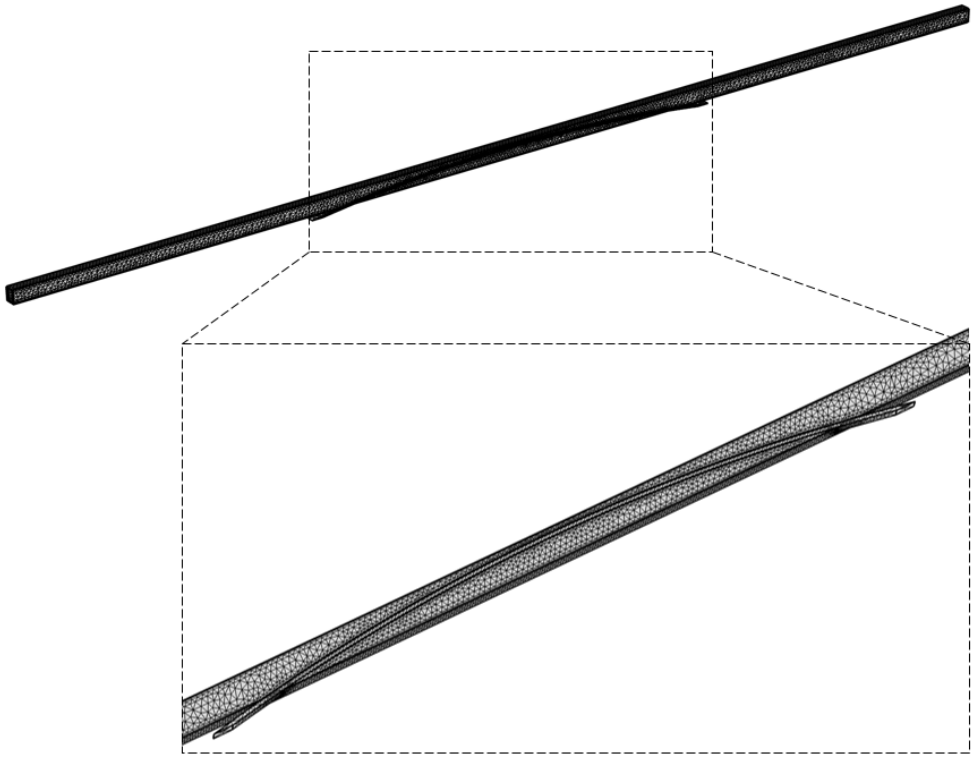

Fig. 6.9 3D Mesh Structure

6.2.5 Solver Configuration

A problem is said to be a nonlinear problem if any coefficient or material property contains a dependent variable. The single phase flow interface is always a nonlinear problem unless $\rho=0$ [40]. A time dependent solver is used to compute the solution of the numerical model over a period of time. A backward Euler method is used due to its robust performance. The most important thing to consider while deciding the appropriate approach to solve the numerical model is to identify the nature of coupling. In a case of a weakly coupled physics, it is easier to treat each physics response sequentially, using the results of the previously solved physics to solve the next physics. This is a very effective

way of reducing computational time with lesser memory requirement. However, this approach is not suitable for this work. A fluid-structure interaction physics is a strongly coupled problem in which deformation of the solid affects the fluid and vice versa. For such an interaction, it is necessary to use a fully coupled approach to solve the involved physics. The fully coupled approach is memory intensive, but very much needed to solve strong interactions which can't be solved independently.

6.3 Results

6.3.1 Pressure differential - A domain probe is used to analyze the response of a sinusoidal pressure differential condition. The pressure differential follows a sinusoidal curve with a frequency of 3Hz as shown in fig. 6.10. Three complete cycles of fluid oscillations are shown in the fig. 6.10. During first half of the cycle, positive pressure differential forces the fluid to follow forward direction, from inlet to outlet. During second half of the cycle, negative pressure differential forces the fluid to follow reverse direction, from outlet to inlet. One complete cycle corresponds to one oscillation across the piezoelectric patch.

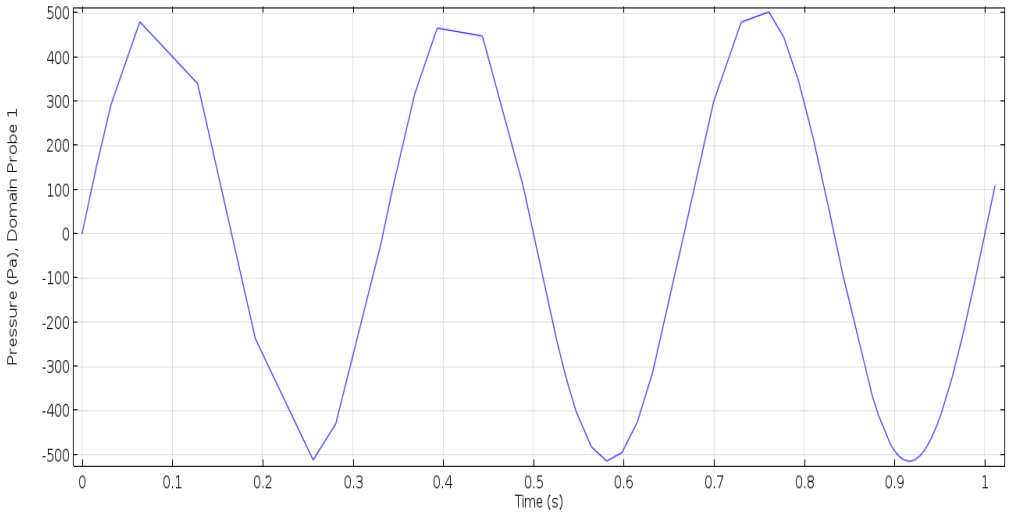

Fig. 6.10 Pressure differential verses time

6.3.2 Positive half cycle of the oscillation- During the first half cycle, fluid travels towards the outlet of the pipe with gradually increasing velocity. At 0.4 seconds, we can observe from fig. 6.10 and 6.11 that the pressure differential is reaching its maximum positive value. At the same instant, it is seen from fig. 6.12 that the velocity is also approaching its maximum value with the flow flowing in the forward direction as shown in fig. 6.13. At the fluid-structure interaction boundaries, fluid velocity is considered to be equal to solid velocity and stress generated in the piezoelectric patch can be seen in 6.14. In the figure 6.14, we can observe that the piezoelectric patch is getting deformed under the fluid pressure as indicated by path lines. Path lines indicate the direction of deformation of the solid.

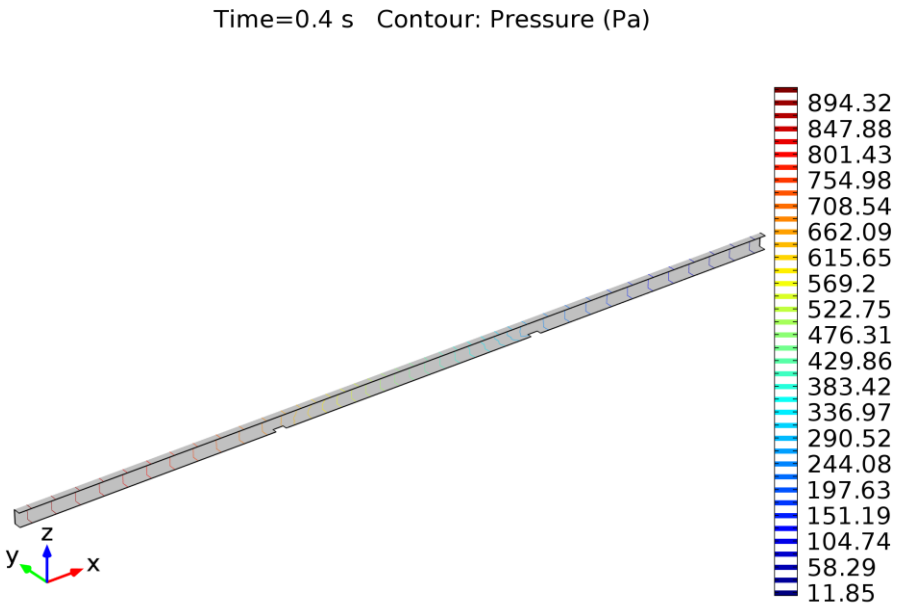

Fig. 6.11. Pressure contour at 0.4 seconds

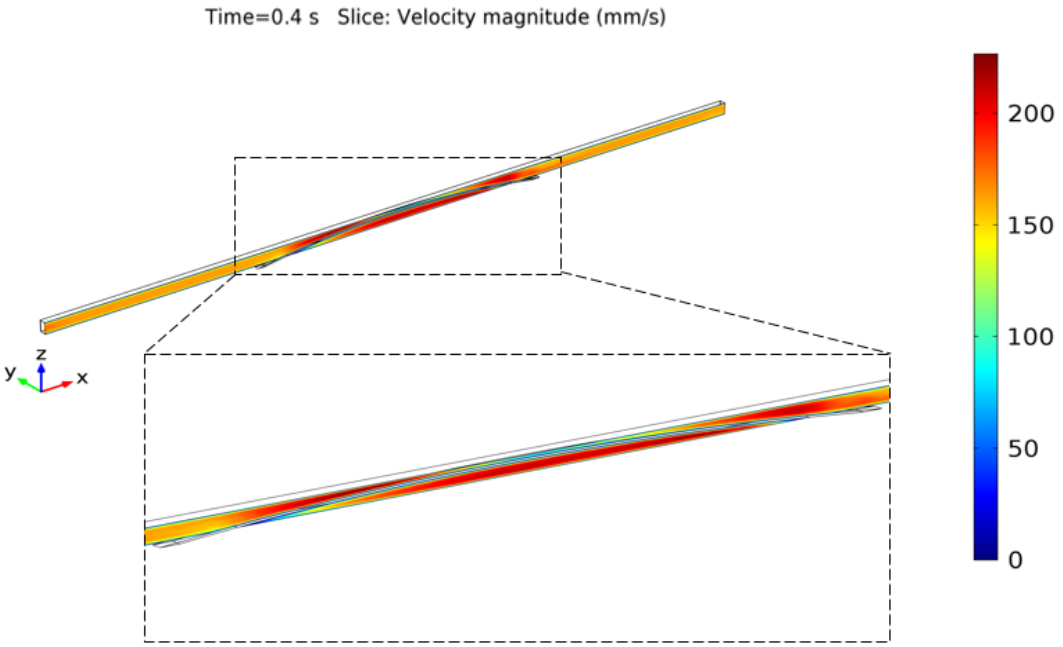

Fig 6.12 Velocity of forward flowing fluid

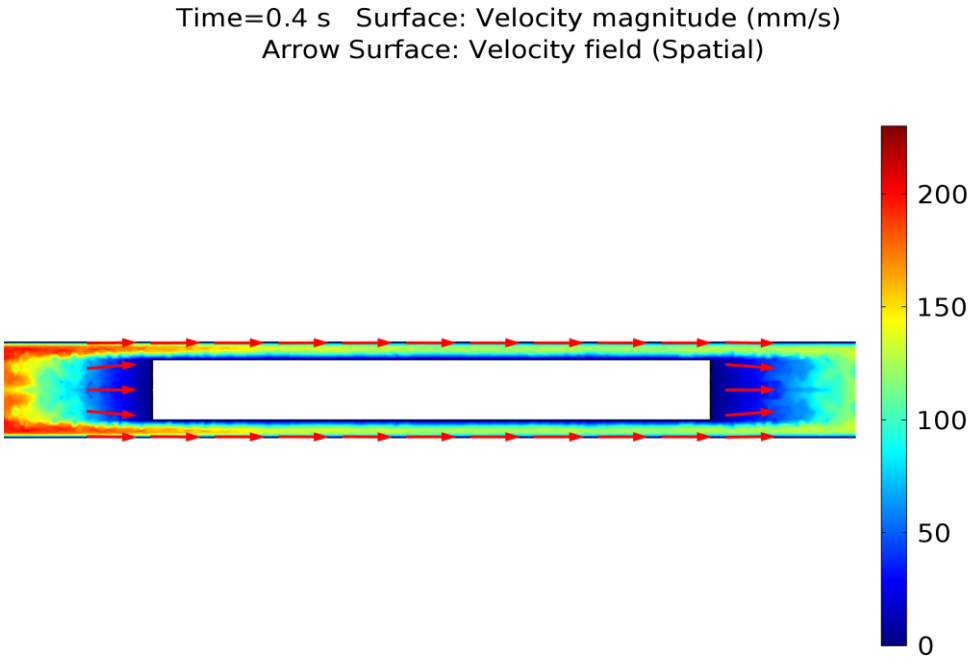

Fig 6.13 Path lines showing of direction of the fluid flow

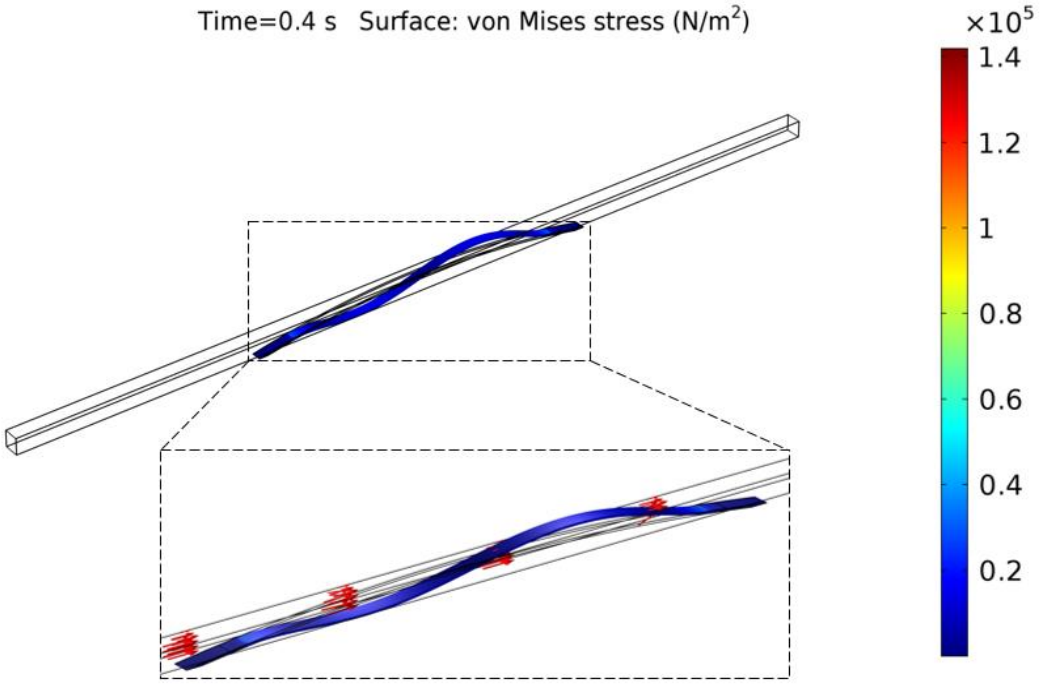

Fig 6.14 Stress field in the piezoelectric patch during forward fluid flow

6.3.3 Negative half cycle of the oscillation- During second half of the cycle, due to negative pressure differential, fluid starts flowing in the reverse direction as shown in fig 6.15 and 6.16. Reversed fluid flow direction deforms the piezoelectric patch as shown in fig. 6.17. Fluid exerts maximum surface pressure on the right side of the patch causing it to deform more in the downward direction as shown in fig 6.18.

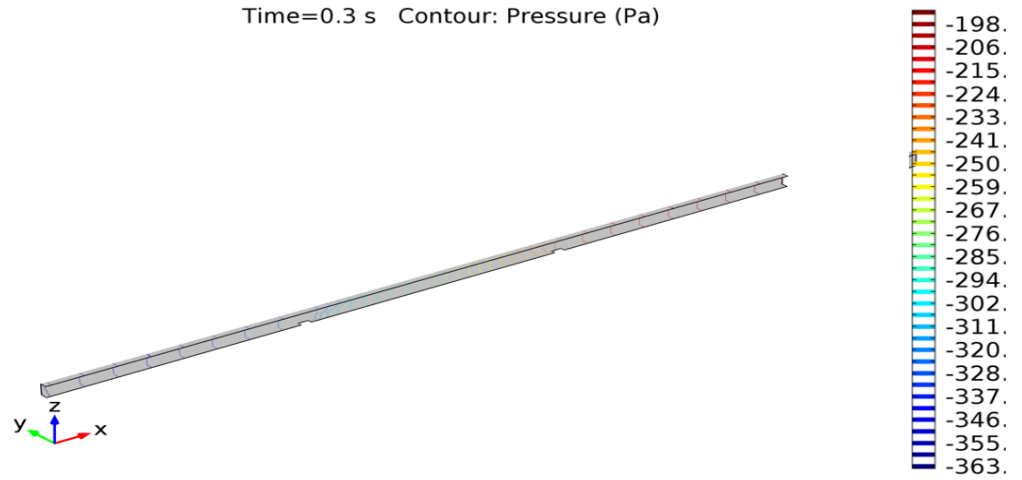

Fig. 6.15 Pressure contour during reverse fluid flow

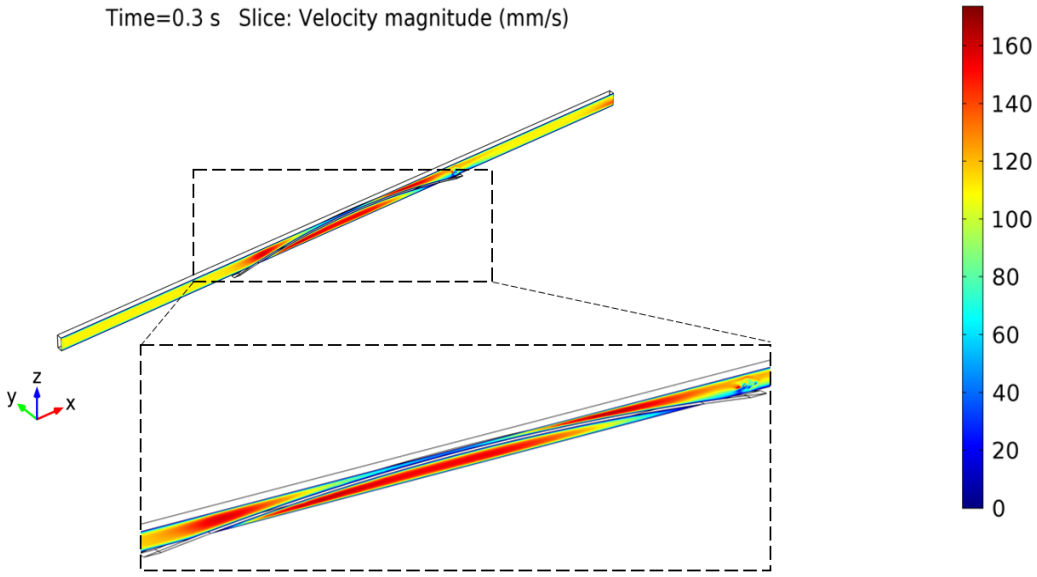

Fig 6.16 Velocity of reverse flowing fluid

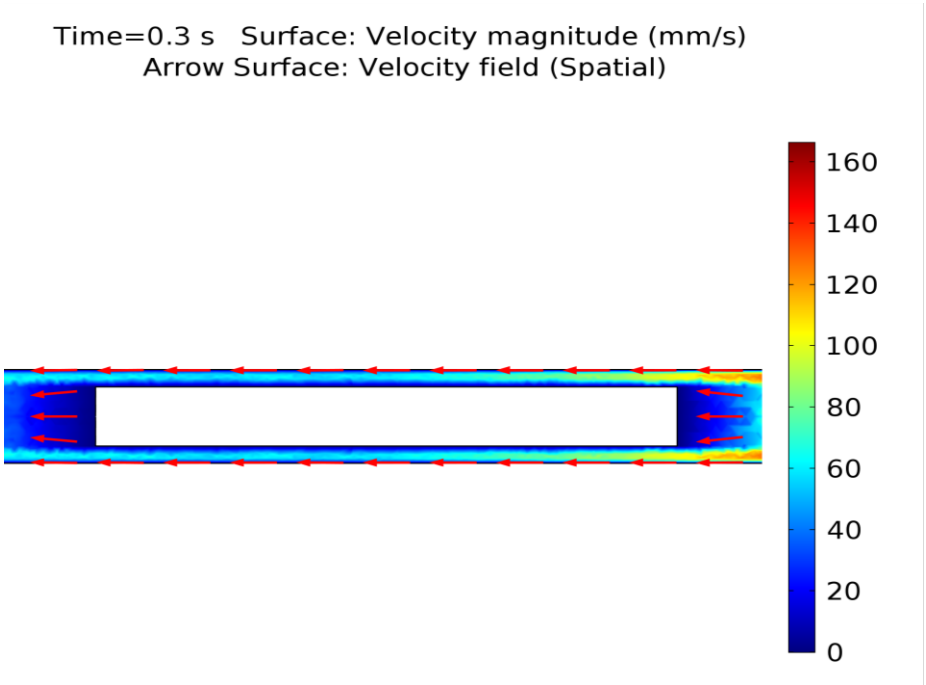

Fig 6.17 Path lines showing of direction of the fluid flow

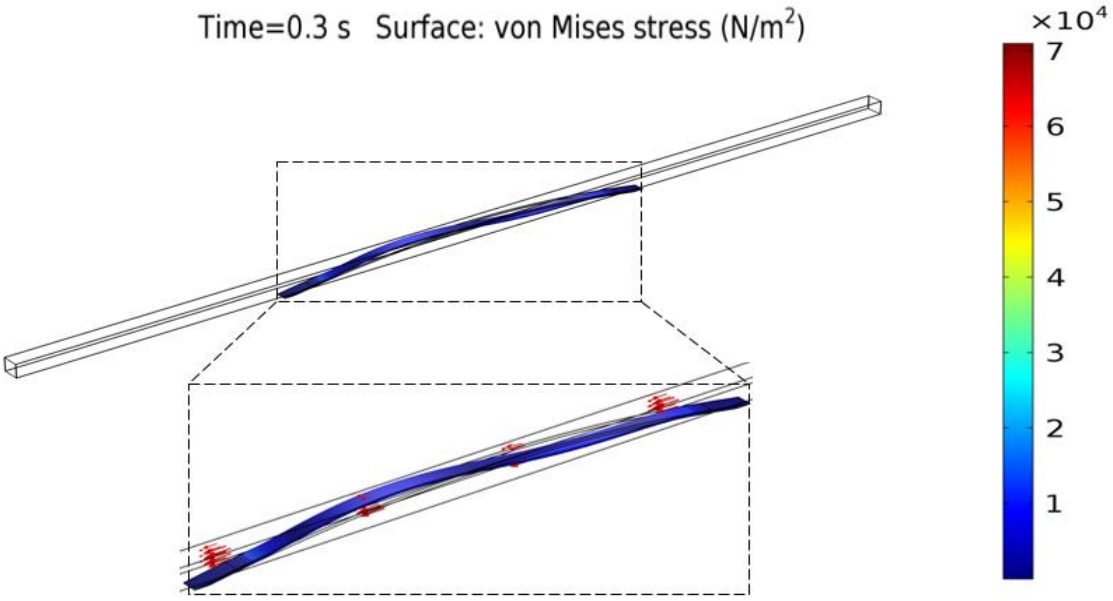

Fig 6.18 Stress field in the piezoelectric patch during reverse fluid flow

6.3.4 Voltage verses time response-

Experimental set up - Voltage data recorded was recorded by experiments as explained in section 4.2.3. Time dependent oscillations in the voltage behavior were significantly observed for heat input starting from 250W. Voltage verses time data recorded for 2 seconds is shown in fig. 6.19.

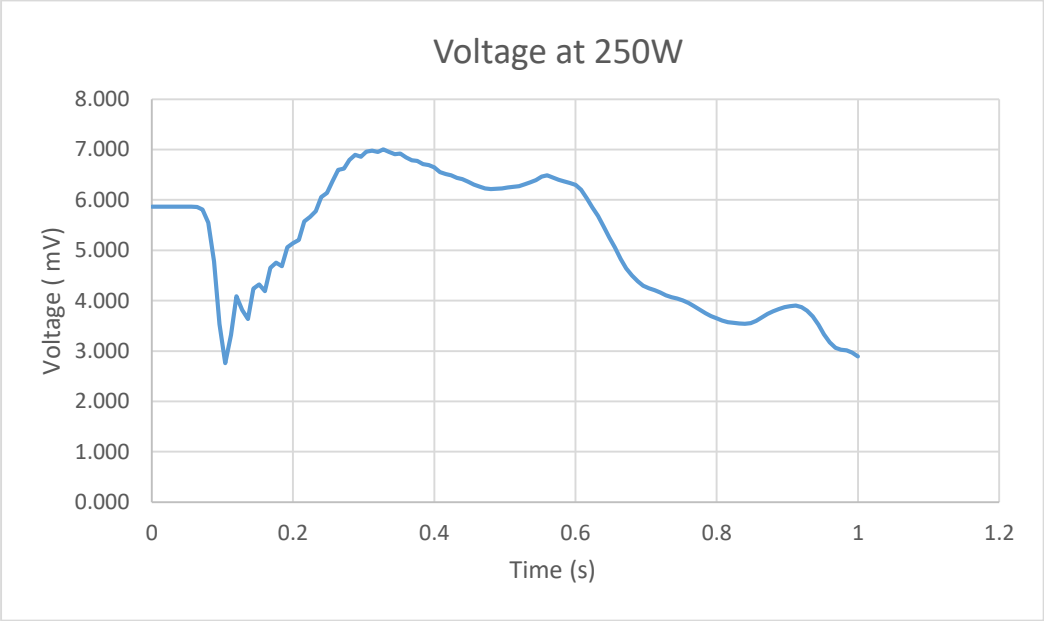

Fig. 6.19 Experimental voltage for 250W heat input

Numerical model – In the numerical model, voltage was calculated using electrostatic physics based on stress generated in the piezoelectric patch. Voltage verses time data is of utmost importance in this research, as it can be used to study feasibility of the proposed concept. It can also be used to optimize the OHP parameters and heat input based on the required voltage output and power requirement. Developed numerical model aids in analyzing effect of input parameters on output voltage and provides a means to study

capability of the proposed system for the energy harvesting purpose. Voltage generated by the piezoelectric patch in the numerical model is shown in fig. 6.20

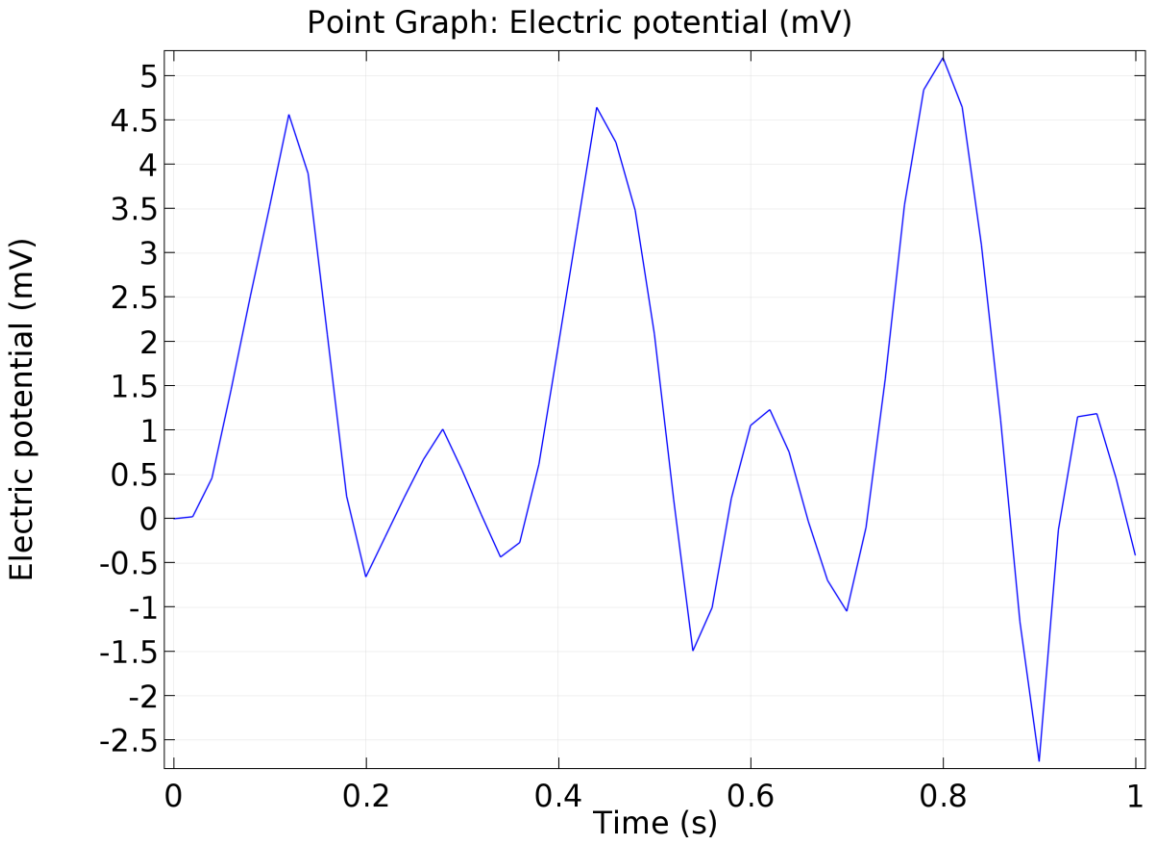

Fig. 6.20 Voltage verses time plot by numerical model

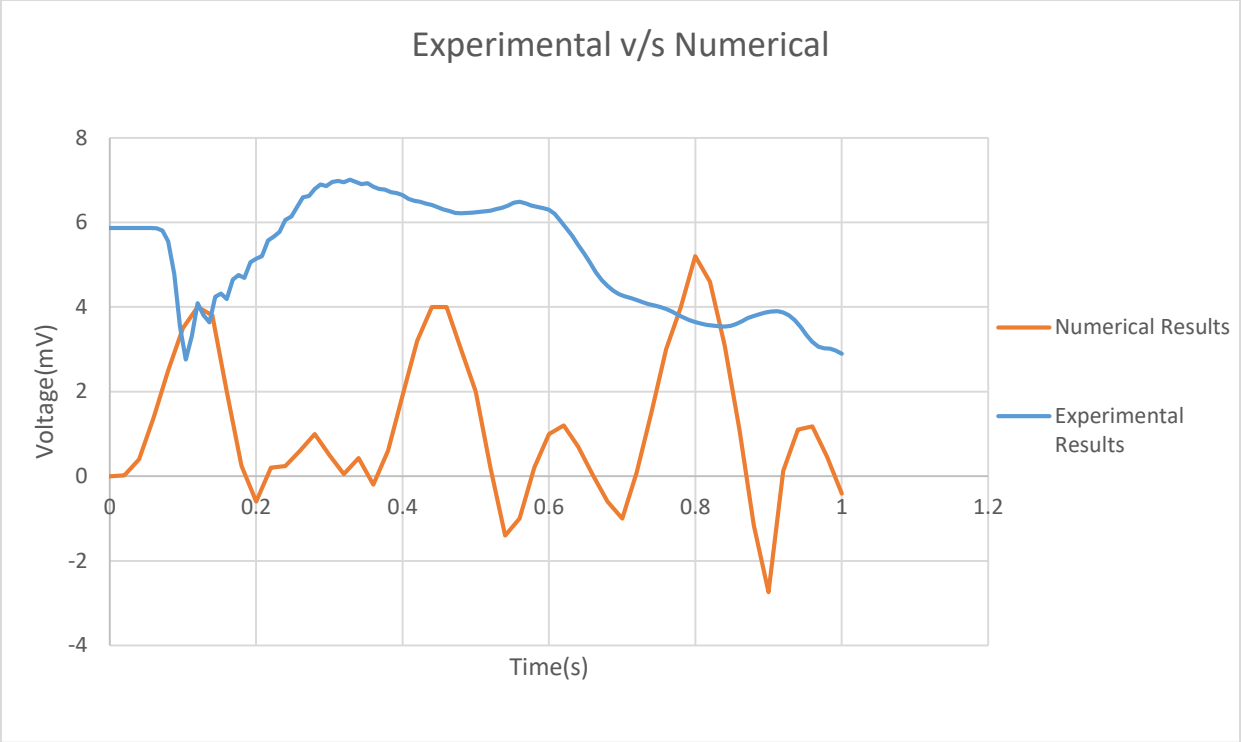

Fig 6.21 Comparison of voltage

We can see in the fig. 6.21, the peak value of voltage predicted by numerical model is ~5mV. The peak value of voltage recorded by experimental measurements is ~7mV. We can find the quantitative agreement in the value of peak voltage predicted by the developed numerical model. However, there is difference in the behavioral trend observed in both cases. The difference can be attributed to various reasons. In the OHP, the oscillating flow depends on multiple factors as explained in section 2.2.2. Changes in any of the listed parameters can affect the pressure distribution inside the OHP resulting in significant changes in the flow pattern. In this work, pressure differential is calculated based on an assumption that there are no irregularities in the OHP parameter data which serves as an input for the calculation. Capturing all the parameters in experiments needs extensive data

measurement technology. Hence, it is challenging to replicate exact dynamic behavior of the OHP which is susceptible to several changes. However, with the use of the developed numerical model, it is possible to get an estimate of the range of voltage values based on the given heat input. With an extensive and detailed collection of OHP operating parameters, it is possible to get the non-uniform pressure distribution specific to the OPH operating condition.

Another important reason of irregularity in the trend is exclusion of electrical circuit physics. Experimentally, the voltage data is measured using a sophisticated circuitry consisting of a DAQ system which uses a low pass frequency filter. Due to the presence of this filter, only positive peaks of voltage are recorded filtering the negative peaks. This results in the wave form as shown in the fig. 6.30. A complete electrical circuit attached with the electrostatics physics will result in estimating the voltage data with more accuracy.

Various measures helpful to limit the variations in the results are discussed in the chapter 7.

CHAPTER SEVEN

CONCLUSIONS AND FUTURE WORK

7.1 Contribution of the current research work

In this research, the main focus was to develop a multi-physics numerical analysis model that aids in estimating the electrical potential developed by the energy harvesting system. An independent analysis was done to calculate the pressure differential value inherent to oscillating heat pipe under investigation. Proposed multi physics numerical model consists of a three-way interaction between fluid flow, solid mechanics and electrostatics physics which are coupled together using fluid-structure interface and piezoelectricity coupling. The range of electric potential predicted by the simulations fall in the similar range as recorded by experiments, hence verifying the validity of the model. There is a variation observed in the voltage behavioral trend of simulation results. The reasons of these variations are investigated and can be considered as future research expansion opportunities as explained later in this chapter.

7.2 Conclusions

1. Energy harvesting process using oscillating heat pipe and piezoelectric assembly provides an opportunity to harvest waste heat energy into electrical energy.
2. Numerical model developed to estimate voltage of the system needs to consider thermo-hydrodynamic interaction, fluid-structure interaction and piezoelectric physics. Multi physics coupling is used to fully capture the effect of heat input on

the oscillating fluid flow which is responsible for stress generation in the piezoelectric patch.

3. A non-uniform pressure differential in the OHP is responsible for the generation of the oscillatory flow. Pressure differential depends upon various parameters such as heat transfer properties of the working fluid, OHP operating conditions, OHP geometric properties, etc. This equation can be expressed as given in eq. 37.
4. With the heat input of 250W, electrical potential was generated in the range of 5-10 mV. Opportunity of increasing the electrical energy output lies in optimal placement, geometry, and material properties of the piezoelectric patch. Efficiency of the system can also be enhanced by achieving optimal operating conditions of the OHP and by maintaining the pressure condition of the OHP in such a way that fluid oscillation frequency matches with resonance frequency of the piezoelectric patch.

7.3 Recommendations for Future Research

The difference in results can be attributed to limitations in gathering experimental OHP operating parameter data as well as limitations of the numerical model. Considering the sophisticated equipment required to measure fluid parameters such as pressure, flow rate and fluid velocity for a particular heat input in the OHP, it was not possible to collect extensive data required to formulate a semi-empirical model of the OHP parameters. An independent investigation done on thermo-hydrodynamic interaction assists in studying pressure differential trend observed in OHP. However, it can’t estimate exact dynamic pressure response of the system. Various ways of measuring the pressure response of the

OHP can be implemented in the future work of the research [55][56]. In the experimental setup, various thermocouples are inserted in the OHP tube to measure temperature of the working fluid. This causes an obstruction to the fluid flow resulting in variable flow rate and fluid velocity profile. It is necessary to analyze the effect of the obstruction to the fluid flow to get accurate pressure boundary condition.

The lack of pressure data being the prime reason for variation in the predicated voltage by the numerical model, another important reason is the single-phase fluid flow considered in fluid flow physics. The fluid flow in the OHP consists of liquid-vapor phase of the fluid, making it a multi-phase flow. However, single –phase flow consisting liquid phase of water was considered in the simulation. This consideration as based on the experimental finding which showed that the region around piezoelectric patch consist of water predominantly in liquid form. Due to the lack of multi-phase flow, the effect of fill ratio of the OHP can't be demonstrated using the numerical model. Reynolds's number for the observed fluid flow falls in the transient region. Future work can look into building a turbulent multi-phase flow model to depict exact experimental condition.

Future work of this research will look into optimizing piezoelectric placement and geometric parameters to enhance performance and increase power output of the system. In this work, only a harvester section was modeled concerning area around piezoelectric patch under investigation. A numerical model consisting an entire assembly of OHP with piezoelectric patch will aid in studying the coupling of all involved physics with more closely and accurately [57][58].

REFERENCES

[1] S. Priya and D. J. Inman, “Energy harvesting technologies,” *Energy Harvest. Technol.*, pp. 1–517, 2009.

[2] H. B. Ma *et al.*, “Effect of nanofluid on the heat transport capability in an oscillating heat pipe,” *Appl. Phys. Lett.*, vol. 88, no. 14, pp. 1–7, 2006.

[3] Paradiso, Joseph A., and Thad Starner. "Energy scavenging for mobile and wireless electronics." IEEE Pervasive computing 4.1 (2005): 18-27.

[4] S. R. Anton and H. A. Sodano, “A review of power harvesting using piezoelectric materials (2003–2006),” *Smart Mater. Struct.*, vol. 16, no. 3, pp. R1–R21, 2007.

[5] P. Glynne-Jones, M. J. Tudor, S. P. Beeby, and N. M. White, “An electromagnetic, vibration-powered generator for intelligent sensor systems,” *Sensors Actuators, A Phys.*, vol. 110, no. 1–3, pp. 344–349, 2004.

[6] P. D. Mitcheson, P. Miao, B. H. Stark, E. M. Yeatman, A. S. Holmes, and T. C. Green, “MEMS electrostatic micropower generator for low frequency operation,” *Sensors Actuators, A Phys.*, vol. 115, no. 2–3 SPEC. ISS., pp. 523–529, 2004.

[7] R. D. Kornbluh *et al.*, “<title>Electroelastomers: applications of dielectric elastomer transducers for actuation, generation, and smart structures</title>,” vol. 4698, pp. 254–270, 2002.

[8] H. A. Sodano, “Comparison of Piezoelectric Energy Harvesting Devices for Recharging Batteries,” *J. Intell. Mater. Syst. Struct.*, vol. 16, no. 10, pp. 799–807, 2005.

[9] H. A. Sodano, G. Park, and D. J. Inman, “An investigation into the performance of macro-fiber composites for sensing and structural vibration applications,” *Mech. Syst. Signal Process.*, vol. 18, no. 3, pp. 683–697, 2004.

[10] Y. Yang, L. Tang, and H. Li, “Vibration energy harvesting using macro-fiber composites,” *Smart Mater. Struct.*, vol. 18, no. 11, p. 115025, 2009.

[11] S. Roundy, P. K. Wright, and J. Rabaey, “A study of low level vibrations as a power source for wireless sensor nodes,” *Comput. Commun.*, vol. 26, no. 11, pp. 1131–1144, 2003.

[12] S. Roundy, “On the Effectiveness of Vibration-based Energy Harvesting,” *J. Intell. Mater. Syst. Struct.*, vol. 16, no. 10, pp. 809–823, 2005.

[13] S. Roundy and Y. Zhang, “Toward self-tuning adaptive vibration-based microgenerators,” vol. 5649, p. 373, 2005.

[14] P. Niu, P. Chapman, R. Riemer, and X. Zhang, “Evaluation of motions and actuation methods for biomechanical energy harvesting,” *PESC Rec. - IEEE Annu. Power Electron. Spec. Conf.*, vol. 3, no. July, pp. 2100–2106, 2004.

[15] L. Mateu, “Optimum Piezoelectric Bending Beam Structures for Energy Harvesting using Shoe Inserts,” *J. Intell. Mater. Syst. Struct.*, vol. 16, no. 10, pp. 835–845, 2005.

[16] N. S. Shenck and J. A. Paradiso, “Energy scavenging with shoe-mounted piezoelectrics,” *IEEE Micro*, vol. 21, no. 3, pp. 30–42, 2001.

[17] B. P. D. Mitcheson *et al.*, “¬¬¬MUST REVIEW-Human and Machine Motion for Wireless Electronic Devices,” vol. 96, no. 9, pp. 1457–1486, 2008.

[18] G. Acciani, F. Adamo, F. Di Modugno, and G. Gelao, “Modeling and simulation of cantilever beam for wind energy harvesting,” *J. Vibroengineering*, vol. 18, no. 2, 2016.

[19] S. Priya, “Modeling of electric energy harvesting using piezoelectric windmill,” *Appl. Phys. Lett.*, vol. 87, no. 18, pp. 1–3, 2005.

[20] I. Kuehne, A. Van Der Linden, J. Seidel, M. Schreiter, L. Fromme, and A. Frey, “FLUID-STRUCTURE INTERACTION MODELING FOR AN OPTIMIZED DESIGN OF A PIEZOELECTRIC ENERGY HARVESTING MEMS GENERATOR Siemens AG , Corporate Technology , Corporate Research & Technologies , Munich , Germany Comsol Multiphysics GmbH , Göttingen , Germany FLUID-,” pp. 1–4, 2011.

[21] G. W. Taylor, J. R. Burns, S. M. Kammann, W. B. Powers, and T. R. Welsh, “The energy harvesting Eel: A small subsurface ocean/river power generator,” *IEEE J. Ocean. Eng.*, vol. 26, no. 4, pp. 539–547, 2001.

[22] Y. Xia, S. Michelin, and O. Doaré, “Fluid-solid-electric lock-in of energy-harvesting piezoelectric flags,” *Phys. Rev. Appl.*, vol. 3, no. 1, 2015.

[23] M. Zhang, Y. Liu, and Z. Cao, “Modeling of piezoelectric energy harvesting from freely oscillating cylinders in water flow,” *Math. Probl. Eng.*, vol. 2014, 2014.

[24] M. R. Sarker, A. Mohamed, and R. Mohamed, “Cantilever beam vibration from fluid interactions with triangular shape blunt body for energy harvesting application,” *2015 IEEE Student Conf. Res. Dev. SCOReD 2015*, no. Viv, pp. 6–10, 2016.

[25] H. D. Akaydin, N. Elvin, and Y. Andreopoulos, “Energy Harvesting from Highly Unsteady Fluid Flows using Piezoelectric Materials,” *J. Intell. Mater. Syst. Struct.*, vol. 21, no. 13, pp. 1263–1278, 2010.

[26] K. A. Cunefare, E. A. Skow, A. Erturk, J. Savor, N. Verma, and M. R. Cacan, “Energy harvesting from hydraulic pressure fluctuations,” *Smart Mater. Struct.*, vol. 22, no. 2, p. 25036, 2013.

[27] J. Lebet, Living on Air—"History of the ATMOS Clock, Jaeger-LeCoultre, 1997.”

[28] M. Kishi *et al.*, “Micro thermoelectric modules and their application to wristwatches as an energy source,” *Eighteenth Int. Conf. Thermoelectr. Proceedings, ICT’99 (Cat. No.99TH8407)*, no. 1 999, pp. 301–307.

[29] N. S. Hudak and G. G. Amatucci, “Small-scale energy harvesting through thermoelectric, vibration, and radiofrequency power conversion,” *J. Appl. Phys.*, vol. 103, no. 10, 2008.

[30] S. Rahman, “Green power: what is it and where can we find it?,” *IEEE Power Energy Mag.*, vol. 1, no. 1, pp. 30–37, 2003.

[31] Akachi, Hisateru. "Structure of a heat pipe." U.S. Patent No. 4,921,041. 1 May 1990.

[32] O. Heat, P. For, W. Heat, R. In, and H. Systems, “IMECE2015-52720,” pp. 1–7, 2017.

[33] S. Rittidech, W. Dangeton, and S. Soponronnarit, “Closed-ended oscillating heat-pipe (CEOHP) air-preheater for energy thrift in a dryer,” *Appl. Energy*, vol. 81, no. 2, pp. 198–208, 2005.

[34] S. Rittidech and S. Wannapakne, “Experimental study of the performance of a solar collector by closed-end oscillating heat pipe (CEOHP),” *Appl. Therm. Eng.*, vol. 27, no. 11–12, pp. 1978–1985, 2007.

[35] Y. Zhang and A. Faghri, “Advances and Unsolved Issues in Pulsating Heat Pipes,” *Heat Transf. Eng.*, vol. 29, no. 1, pp. 20–44, 2008.

[36] B. Taft and F. Laun, “Experimental Investigation of in Situ Pressure Measurement of an Oscillating Heat Pipe,” *Front. Heat Pipes*, vol. 5.1, 2014.

[37] Reay, David, Ryan McGlen, and Peter Kew. Heat pipes: theory, design and applications. Butterworth-Heinemann, 2013

[38] S. Khandekar, P. Charoensawan, M. Groll, and P. Terdtoon, “Closed loop pulsating heat pipes - Part B: Visualization and semi-empirical modeling,” *Appl. Therm. Eng.*, vol. 23, no. 16, pp. 2021–2033, 2003.

[39] Temam, Roger. Navier-stokes equations. Vol. 2. Amsterdam: North-Holland, 1984

[40] P. Interface and B. User, “C omsol Multiphysics,” *Interface*, 2012.

[41] Erturk, Alper, and Daniel J. Inman. Piezoelectric energy harvesting. John Wiley & Sons, 2011.

[42] T. Ikeda, “Fundamentals of Piezoelectricity,” *Piezoelectric Transducers Vib. Control Damping*, pp. 9–35, 1990.

[43] S. . Monroe, J.G., Bhandari, M., Fairley, J., Myers, O.J., Shamsaei, N., Thompson, “Energy Harvesting via Thermo-Piezoelectric Transduction within a Heated Capillary,” *Appl. Phys. Lett.*, 2017.

[44] M. B. Shafii, A. Faghri, and Y. Zhang, “Thermal Modeling of Unlooped and

Looped Pulsating Heat Pipes," *J. Heat Transfer*, vol. 123, no. 6, p. 1159, 2001.

[45] Y. Zhang, A. Faghri, and M. B. Shafii, "Analysis of liquid-vapor pulsating flow in a U-shaped miniature tube," *Int. J. Heat Mass Transf.*, vol. 45, no. 12, pp. 2501–2508, 2002.

[46] Y. Zhang, "Oscillatory Flow in Pulsating Heat Pipes," vol. 17, no. 3, pp. 1–10, 2003.

[47] Z. Li, M. Yang, Y. Zhang, and S. Montgomery-smith, "Investigation of Oscillatory Flow in an Oscillating Heat Pipe With," vol. 22, no. 6, pp. 485–502, 2015.

[48] P. Applications, "What is a Macro Fiber Composite ?," *Technology*.

[49] K. Steiger and P. Mokrý, "Finite element analysis of the macro fiber composite actuator: macroscopic elastic and piezoelectric properties and active control thereof by means of negative capacitance shunt circuit," *Smart Mater. Struct.*, vol. 24, no. 2, p. 25026, 2015.

[50] X. Liu, Q. Sun, C. Zhang, and L. Wu, "High-Speed Visual Analysis of Fluid Flow and Heat Transfer in Oscillating Heat Pipes with Different Diameters," *Appl. Sci.*, vol. 6, no. 11, p. 321, 2016.

[51] G. Nader, E. Silva, and J. Adamowski, "Effective damping value of piezoelectric transducers determined by experimental techniques and numerical analysis," *ABCM Symp. Ser. Mechatronics*, vol. 1, pp. 271–279, 2004.

[52] COMSOL, "The Structural Mechanics Module User's Guide," no. 1215, pp. 137–150, 2012.

[53] A. M. González, Á. García, C. Benavente-Peces, and L. Pardo, "Revisiting the

characterization of the losses in piezoelectric materials from impedance spectroscopy at resonance," *Materials (Basel).*, vol. 9, no. 2, 2016.

[54] M. E. (Morgan Electroceramics), "PZT500 Series," *Datasheet http://www.morganelectroceramics.com/materials/soft-pzt/*, no. 286773, pp. 10–11, 2013.

[55] Y. Park, M. R. Tanshen, M. J. Nine, H. Chung, and H. Jeong, "Characterizing pressure fluctuation into single-loop oscillating heat pipe," *J. Cent. South Univ.*, vol. 19, no. 9, pp. 2578–2583, 2012.

[56] S. Sangiamsuk, B. Bubphachot, O. Watanabe, and S. Rittidech, "Measurement of internal pressure and thermal performance in a closed-loop oscillating heat-pipe with check valves (CLOHP / CV)," vol. 52, no. August, pp. 531–540, 2014.

[57] R. C. Givler and M. J. Martinez, "Modeling of Pulsating Heat Pipes," *Distribution*, no. August, p. 33, 2009.

[58] S. Khandekar, S. Manyam, M. Groll, and M. Pandey, "Two-phase flow modeling in closed loop pulsating heat pipes," *13th IHPC*, vol. 6, pp. 0–7, 2004.